

Louisiana Tech University

Louisiana Tech Digital Commons

Master's Theses

Graduate School

Spring 5-25-2024

Comparing Proliferation Rates and Collagen Production of Cells Treated with CuHARS

Katie Elizabeth McKenzie

Follow this and additional works at: <https://digitalcommons.latech.edu/theses>



Part of the [Biomedical Engineering and Bioengineering Commons](#), and the [Chemistry Commons](#)

**Comparing Proliferation Rates and Collagen
Production of Cells Treated with CuHARS**

by

Katie McKenzie BS

A Thesis Presented in Partial Fulfillment
of the Requirements of the Degree
Master of Science

COLLEGE OF ENGINEERING AND SCIENCE
LOUISIANA TECH UNIVERSITY

May 2024

LOUISIANA TECH UNIVERSITY

GRADUATE SCHOOL

April 2, 2024

Date of thesis defense

We hereby recommend that the thesis prepared by

Katie McKenzie

entitled **Comparing Proliferation Rates and Collagen Production of Cells**

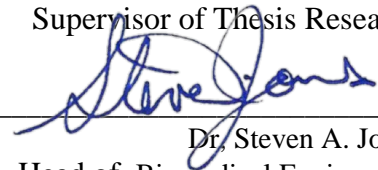
Treated with CuHARS

be accepted in partial fulfillment of the requirements for the degree of

Master of Science in Engineering, Biomedical Engineering Concentration



Dr. Mark DeCoster
Supervisor of Thesis Research



Dr. Steven A. Jones
Head of Biomedical Engineering

Thesis Committee Members:

Dr. Steven A. Jones

Dr. Mary Caldorera-Moore

Approved:



Collin Wick
Dean of Engineering & Science

Approved:



Ramu Ramachandran
Dean of the Graduate School

ABSTRACT

Cartilage is the padding in joints that protects the bones and aids in motion. Problems with the cartilage in the knee can be caused by mechanical damage or diseases like osteoarthritis. Chondrocytes make cartilage. The objective of this study is to determine the doubling time of chondrocytes per passage. I also want to determine the base amount of collagen-II created by chondrocytes as they age. I also want to determine how long it takes CuHARS to break down in different cell medias.

Chondrocytes, human dermal fibroblasts, and CRL 2303 cells were grown and cultured for over a year. During that time, media was collected for a collagen assay, and the cells were imaged mid-passage to determine the doubling time. Also, CuHARS were mixed with cell media to determine the time required for the material to break down in the media.

Cell growth rates were inconsistent. CRLs make less collagen as they age. Results on collagen production by HDFs were inconclusive. Treated chondrocytes may make more collagen than untreated chondrocytes, but more testing is necessary.

Ultimately, much more experimentation is necessary. CRL 2303 cells appear to make less collagen as they age. Human dermal fibroblasts need much more experimentation. Treated chondrocytes initially make more collagen than untreated ones.

APPROVAL FOR SCHOLARLY DISSEMINATION

The author grants to the Prescott Memorial Library of Louisiana Tech University the right to reproduce, by appropriate methods, upon request, any, or all portions of this Thesis. It is understood that “proper request” consists of the agreement, on the part of the requesting party, that said reproduction is for his personal use and that subsequent reproduction will not occur without written approval of the author of this Thesis. Further, any portions of the Thesis used in books, papers, and other works must be appropriately referenced to this Thesis.

Finally, the author of this Thesis reserves the right to publish freely, in the literature, at any time, any or all portions of this Thesis.

Author _____

Date _____

DEDICATION

This document is dedicated to all the aspiring engineers who never thought they would be able to achieve their wildest dreams. Especially young Katie, you were so full of doubt, but you have so much greatness ahead of you.

TABLE OF CONTENTS

ABSTRACT.....	iii
APPROVAL FOR SCHOLARLY DISSEMINATION	iv
DEDICATION	v
LIST OF FIGURES	ix
LIST OF TABLES	xi
ACKNOWLEDGMENTS	xii
CHAPTER 1 INTRODUCTION	1
1.1 Copper.....	1
1.2 Collagen	1
1.3 Alternative cell types	2
1.4 Research Goals	2
CHAPTER 2 BACKGROUND	3
2.1 Overview.....	3
2.2 Proliferation	5
2.2.1 General Cell Proliferation.....	5
2.2.2 Growth Factors on Cell Proliferation.....	6
2.3 Collagen	7
2.4 Copper.....	10
2.4.1 CuHARS	10
CuHARS Breakdown.....	11
2.5 Other Cell Types.....	12

2.5.1	Human Mesenchymal Stem Cells	12
2.5.2	Astrocytes:	12
2.5.3	Human Dermal Fibroblasts	13
2.5.4	CRL 2303.....	13
2.6	Research Need	14
2.7	Hypotheses.....	14
CHAPTER 3 METHODS		15
3.1	Treating Cells with CuHARS:	15
3.2	Cell Culture.....	15
3.3	Cell Counting Procedure:.....	16
3.3.1	Hemocytometer	16
3.3.2	Hemocytometer Control.....	19
3.3.3	Counting cells in between passages	20
3.3.4	HDFs.....	23
3.3.5	CRL2303.....	23
3.3.6	Accuracy	23
3.4	Collagen Assay	24
3.4.1	Protocol.....	24
3.4.2	Analysis.....	26
3.4.3	Accuracy	26
3.5	CuHARS Breakdown.....	27
CHAPTER 4 RESULTS		30
4.1	CuHARS Breakdown.....	31
4.2	Proliferation	38
4.3	Collagen Assay	43

CHAPTER 5 DISCUSSION.....	48
CHAPTER 6 CONCLUSIONS AND FUTURE WORK.....	54
6.1 Conclusions.....	54
6.2 Future Work.....	55
BIBLIOGRAPHY	57
APPENDIX A RStudio Code	64
APPENDIX B MATLAB code for CuHARS breakdown	65
APPENDIX C Astrocyte and Chondrocyte CuHARS Breakdown Plots.....	66

LIST OF FIGURES

Figure 2-1: Structure of Collagen Type II ⁴⁰	7
Figure 2-2: Structure of Collagen Type I. ⁴³	8
Figure 2-3: SEM of cross-section of collagen in a tendon. Scale Bar: 50µm. ⁴⁶	9
Figure 2-4: Brightfield image of CuHARS at 100x Magnification. Scale bar = 100µm.	11
Figure 3-1: Layout of the hemacytometer with the relevant section outlined in red. ⁶⁹ ..	17
Figure 3-2: View of the hemacytometer with stained cells on it, showing high viability as no cells are stained blue.	18
Figure 3-3: Original on the left and greyscale on the right of P10 Chondros.....	21
Figure 3-4: Enhanced Nuclei of Chondrocytes, showing counting success by CellProfiler.....	22
Figure 4-1: A) CuHARS prior to sonication, B) CuHARS after 5 minutes of sonication.	30
Figure 4-2: A) Day 0 CuHARS B) Day 1 CuHARS	31
Figure 4-3: CuHARS in Astrocyte media at Day 0 (A) and Day 8 (B).....	32
Figure 4-4: CuHARS Breakdown in Astrocyte Media.....	33
Figure 4-5: CuHARS breakdown with Astrocyte and Chondrocyte media with accompanying models.....	34
Figure 4-6: A) Chondrocytes 30 minutes post treatment at 10x, B) 20x.	35
Figure 4-7: A) Chondrocytes 6hr post treatment. B) CuHARS 3 days post treatment....	36
Figure 4-8: Chondrocytes 6 hours post treat 100x (A) and 200x (B).....	36
Figure 4-9: Chondrocytes 6hrs post treatment 200x. Areas of interest are circled in red.	37

Figure 4-10: 6 days post-treatment: A) Control B) Treated.....	38
Figure 4-11: Polystyrene beads on the hemocytometer. The beads are 24 μm in diameter as per vendor specifications.	39
Figure 4-12: A) Greyscale of image with dark spots removed. B) Identified cells, C) Cell outlines, D) Accepted cell amount and accompanying data.	40
Figure 4-13: Greyscale image (Left), and the outlined cells (Right).....	41
Figure 4-14: Bar Chart of Chondrocyte, Treated, and HDF Proliferation as Counted by the Hemacytometer. (* - CellProfiler Count)	42
Figure 4-15: Bar Chart of CRL Proliferation.....	42
Figure 4-16: Calibration Curve of Collagen Assay.	43
Figure 4-17: Fluorescein test at 10, 20, and 30 dilution factors	44
Figure 4-18: Fluorescein Test at Collagen Assay Dilutions	44
Figure 4-19: Collagen Production by CRL Cells.....	45
Figure 4-20: Collagen Production of Human Dermal Fibroblasts.....	46
Figure 4-21: Chondrocyte and Treated Chondrocyte Collagen Production. Two data points were taken for each time point. The error bars are the difference between the two data points, divided by 2.	47

LIST OF TABLES

Table 3-1: Components of Sigma-Aldrich Collagen Assay.....	24
Table 3-2: Collagen Standard Proportions	25
Table 4-1: Time Constants for CuHARS breakdown in Astrocyte and Chondrocyte media.....	35

ACKNOWLEDGMENTS

The author wishes to thank the following for their endless help, guidance, words of advice, and encouragement throughout the past years. Dr. DeCoster, thank you for giving me the opportunity to do research on a topic I could have only dreamed of working on. Dr. Jones, thank you for your never-ending support and guidance. I do not know where I would be if it were not for your office door always being open for me. Dr. Caldorera-Moore, thank you for always being in my corner from my undergraduate days until now. Dr. Megan, thank you for everything, I cannot express in words the benefits your relationship has had on me. Steve, thank you for being there with me through the late nights and moments where I doubted myself, your existence brings me peace and the confidence to conquer my dreams. To my family, thank you for always encouraging me despite having no idea what I was talking about most of the time. To my friends not previously listed, thank you for being a safe harbor when I needed a break from my cells. To my cells, thank you for being hardy and allowing me to learn from you. Thank you to my lab mates for your never-ending help and support. Also, thank you to all the people behind the scenes who helped this document become the best version of itself. Without all of you, I would not have achieved what I have, so thank you.

CHAPTER 1

INTRODUCTION

Cartilage is the collagen-rich padding in joints that protects the bones and aids in motion. For example, the cartilage in the knee, created by chondrocytes is critical to pain-free, fluid movement. Problems with the cartilage in the knee can be caused by mechanical damage or diseases like osteoarthritis. Cartilage is created by a cell known as a chondrocyte. However, cartilage heals poorly in adults.¹

1.1 Copper

Copper is critical to the extracellular matrix of chondrocytes.² Copper is a micronutrient that occurs in foods like shellfish and organ meats.³ It has an estimated bioavailability of 75%, when the body consumes $400 \frac{\mu g}{day}$.³ However, copper toxicity can occur and presents as liver and gastrointestinal damage.³ This study examines the physiological response of chondrocytes to additives like copper high-aspect ratio structures (CuHARS) which were created by the DeCoster lab at Louisiana Tech University.⁴ The study also examines how the CuHARS break down throughout different physiological conditions.

1.2 Collagen

Collagen is a protein that contributes to the extracellular matrix to aid in structure, strength, flexibility and support for joints.^{5,6} Collagen type II, which was discovered at

the end of the 1960s, is the most important for the creation of cartilage.^{5,7} Collagen type II makes up over 90% the collagen composition of cartilage.^{2,8,9}

1.3 Alternative cell types

Collagen is not only created by chondrocytes. It is one of the most prevalent proteins in the body.¹⁰ Therefore, the research analyzed fibroblasts and cancer cells to determine how they compare to chondrocytes in terms of proliferation and collagen creation.

1.4 Research Goals

Articular cartilage resists self-repair, which could be a consequence of either slow proliferation by chondrocytes or low production of collagen by these cells. The current research aimed to determine the doubling time of chondrocytes and the amount of collagen produced by them.

Much research has been conducted into the response of chondrocytes to various growth factors.¹¹ This topic is extremely broad, but the primary interest is the effect on metabolism and secretions of chondrocytes.¹² The current study examines the process by which chondrocytes make type II collagen in an effort to increase the current understanding of the metabolism of chondrocytes and the process by which they make cartilage. This study will in turn provide insight into the pathology of chondrocytes.

CHAPTER 2

BACKGROUND

Cartilage is a critical tissue of the body that works together with bones to form the structural support system of the body.¹³ Articular cartilage is considered to be the most studied.¹³ Articular cartilage is the thin layer connecting the ends of bones that articulate in synovial joints.¹³ It allows for smooth movement of the bones as they move.¹⁴ The articular cartilage in the knee and the elbow is made of hyaline cartilage.¹⁵ The matrix of hyaline cartilage is rich in collagen type II, glycosaminoglycans (GAGs), and water.^{15,16} The cellular component of articular cartilage in the knee is 3-5% with the rest of the volume being ECM.¹⁶ Defects in articular cartilage are difficult to repair because it has low vascularization and it is not connected to the lymphatic system.¹⁷ Cartilage repair ability also decreases with the age of the patient.¹⁷

2.1 Overview

Articular cartilage lessens joint stress and friction on the surface of joints, and when the body is in motion, cyclic forces applied to the joints are up to eight times the body weight.¹⁷ When cartilage degrades, it leads to arthritis or other joint diseases which are the primary cause of human mobility disability.¹³ An effort to repair cartilage defects was initiated in 1987 with the culture and implantation of chondrocytes into humans.¹ In this application, chondrocytes are often stimulated to proliferate more and create more extracellular matrix.¹⁸ Chondrocytes account for only about 1% of the cartilage tissue,

and the rest of the tissue is made up of the extracellular matrix (ECM).¹⁸ The ECM network is the component that handles the mechanical stress of movement by the body.¹⁸

Further studies examine the effect of mechanical stress on chondrocytes in cell culture (*in vitro*).¹⁹ Kelly et al. compared the mechanical properties of cultured chondrocytes and donor chondrocytes, and they concluded that cultured chondrocytes are comparable to donor chondrocytes.²⁰ However, the cultured chondrocytes exhibited higher tension strength when placed under dynamic deformation.²⁰ Middendorf et al. compared the surface characteristics between native cartilage and cultured cartilage and concluded that cultured cartilage and native cartilage are comparable after enough time in culture.²¹ They used type I collagen scaffolding from the company Koken from Tokyo, Japan.²¹ The comparative research indicates that cultured chondrocytes are mechanically similar to chondrocytes in the body in terms of tensile strength, compressive strength, and friction coefficients.^{20,21}

Researchers have studied the benefits of oxygen deprivation of chondrocytes in culture. Oreffo examined the amount of matrix produced by chondrocytes in an oxygen environment below 8% of atmospheric pressure.²² The paper used Alcian blue and Sirius red to quantify the composition of the extracellular matrix.²² Alcian blue stains proteoglycans in general, and the proteoglycan aggrecan specifically, which is plentiful in the collagen matrix.²³ Aggrecan is a proteoglycan that complexes with hyaluronic acid and gives the tissue its ability to withstand high compressive loads.²³ Sirius red stains for collagen, but does not appear to differentiate between different types of collagen.²⁴

2.2 Proliferation

2.2.1 General Cell Proliferation

Cell division is the process by which cells multiply and increase their numbers over time.²⁵ Cellular proliferation is the specific increase in the number of cells present.²⁵ The process by which cells divide, or proliferate, is called mitosis.²⁵ Cell proliferation can be measured through several techniques including various assays or a hemocytometer.²⁶ Hemocytometers are relatively low cost, but the number of cells must be sufficiently large, and the user must be skilled to mitigate error.²⁶ The luminescence assay detects cells from their luminescent signal, which is proportional to the metabolic activity.²⁶ Use of an imaging platform is a relatively new method for cell counting.²⁶ Digitally counting cells involves different types of computer software that count the cells automatically.²⁶

A researcher could also analyze the metabolic activity of cells and extrapolate those data to determine how the cells are proliferating. An MTT (3-(4,5-Dimethylthiazol-2-Yl)-2,5-Diphenyltetrazolium Bromide) assay is a common metabolic assay that detects cell proliferation based on a linear relationship between cell activity and absorbance.²⁷ The MTT assay uses a spectrophotometer to estimate the number of viable cells.²⁸ The Alamar blue assay is similar to the MTT assay in that it is used to measure cytotoxicity and cell proliferation.^{29,30} The Alamar blue assay measures a combination of cytotoxicity, proliferation, and the metabolic response of cells.²⁹ The results of the test are correlated to the proliferation of the cells.²⁹ However, the results of the test do not appear to directly correlate with an exact number of cells within the well being tested.

Cells proliferate at different rates, as can be observed from a comparison of cancerous cells to non-cancerous cells. Cancerous cells are often characterized by their

high proliferation rates.²⁶ Often, a mutation occurs during cell division, allowing a pre-cancer cell to proliferate out of control which may cause it to grow into a dangerous tumor. Non-cancerous cells, however; have cellular mechanisms in place to control proliferation.³¹ Chondrocytes are known to have relatively low proliferation rates in general and in comparison to cancer cells.¹⁷

2.2.2 Growth Factors on Cell Proliferation

Cell proliferation is controlled by growth factors.³² Fibroblast growth factor (FGF) is of particular interest to the research since it can promote the growth and proliferation of both fibroblasts and chondrocytes.³³ FGF also plays a role in tissue repair, making it attractive to the research.³³ However, some research in rats has indicated that FGF decreases the expression of collagen type II.³⁴ In contrast, newer research has indicated that FGF is critical to cartilage homeostasis.³⁵ FGF-2 is produced in the cartilage, and released when the tissue is damaged.³⁵ It is then released into the extracellular signal-related kinase (ERK) pathway which is used for increasing cell proliferation.^{35,36}

Fetal bovine serum (FBS) is used in media as a supplement and is full of growth factors and hormones.^{37,38} However, some ethical concerns arise with FBS.³⁷ To create the serum, blood is required from a calf, and legal regulations appear to be lacking in the United States and the European Union.³⁸ Horse serum appears to lack the same concerns as FBS.³⁷ Yet, because FBS is so rich in growth factors, it remains the most prevalent serum supplement for cell culture media.³⁷

2.3 Collagen

Collagen is a protein that contributes to the extracellular matrix to aid in structure, strength, flexibility and support for joints.^{5,6} At least 27 types of collagen have been discovered and categorized.³⁹ Collagens types I-V are the most common of the protein family that is the most abundant protein in mammals.¹⁰ Collagen is crucial for the cellular matrix, but it is often used in grafts during surgery and cosmetics because of its supposed anti-aging effects.¹⁰ Collagen type II, which was discovered at the end of the 1960s, is the most important for the creation of cartilage.^{5,7} Collagen type II makes up over 90% the collagen composition of cartilage.^{2,8,9} It has a molecular weight of 2488.745 $\frac{\text{g}}{\text{mol}}$.⁴⁰ **Figure 2-1** shows the structure of Collagen type II. Dark circles are carbon, white circles are hydrogen, light blue circles are nitrogen, and red circles are oxygen.

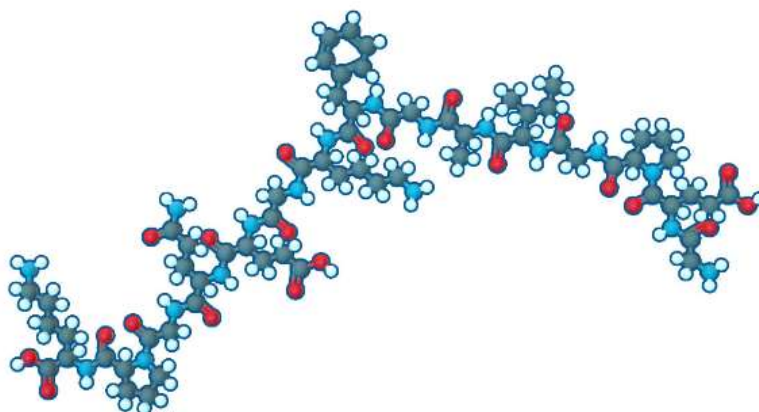


Figure 2-1: Structure of Collagen Type II⁴⁰

Collagen makes up two thirds of the dry weight of cartilage, but little evidence exists as to how much collagen is produced by the cells per passage.⁴¹ Despite the current knowledge that type II is the most important for cartilage generation, collagen type I

devices are the most common in therapeutic research.⁴² **Figure 2-2** shows the structure of type I collagen. It is much straighter than the collagen type II seen in **Figure 2-1**.

Collagen type I weighs a little more than half of type II.^{40,43}

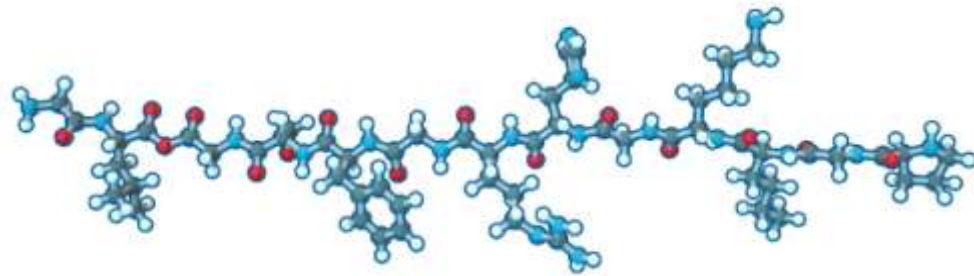


Figure 2-2: Structure of Collagen Type I.⁴³

All types of collagen share similar features of three polypeptide chains formed into a triple helix.³⁹ Type II collagen is shaped like fibrils which are dotted with proteoglycans, glycoproteins, water, and ions, and the components' layout gives cartilage its strength.⁴⁴ The structure of the molecule consists of three α 1-polypeptide chains with a large triple-helix region.⁴⁵ **Figure 2-3** shows that collagen fibrils are rather tightly packed when they form networks of tendons. However, the image does not show that the fibrils form interconnected networks that give the tissue gets its strength.⁴⁶



Figure 2-3: SEM of cross-section of collagen in a tendon. Scale Bar: 50 μ m.⁴⁶

Type II collagen is made by the cells, but it can also be isolated to be used as a dietary supplement.⁷ Osteoarthritis is a crippling disease for those who experience it. Miosge et al. conclude that the progression of osteoarthritis correlates to the increased production of type I collagen.⁴⁷ While type II collagen is still being made, type I collagen appears to override the type II collagen.⁴⁷ Some researchers have experimented with supplementing patients with over-the-counter collagen type II supplements.⁷ The researchers concluded that supplementing type II collagen into the diet was beneficial to the joint pain and quality of life of the patients dealing with knee osteoarthritis.⁷

Assay methods exist to quantify collagen in tissues. The Sircol™ collagen assay, based on Sirius red staining, is one of the most popular assays, but it overestimates the

amount of collagen in the sample because Sirius red also interacts with amino acids of non-collagen proteins.⁴⁸

Fluorescein is a fluorescent agent that can be used to test the instrument that reads fluorescence. It is a yellow substance that is often used in bioimaging for diagnostic purposes.^{49,50} It has a molecular weight of $332.3 \frac{\text{g}}{\text{mol}}$, and it is highly fluorescent even in large dilutions.⁵⁰ It has an excitation peak at 498 nm and an emission peak at 517nm.⁵¹ Fluorescein was used in this study to ensure adequate functioning of the spectrofluorometer.

2.4 Copper

Copper is critical to the extracellular matrix of chondrocytes.² The lysyl oxidase (LOX) family is a group of cuproenzymes that links collagen and elastin to create cartilage.⁵² The LOX family removes the amine group of certain lysine and hydroxylysine residues of collagen, allowing for the covalent bonding of the collagen molecules.^{52,53} Dietary copper is processed in the liver before being attached to apoceruloplasmin, making it into ceruloplasmin.⁵⁴ Research suggests that copper is aided by a carrier protein in the body. Copper enters the cells via protein-mediated transport by high affinity copper uptake protein 1 (hCTR1).^{55,56} However, unknown minor transport mechanisms in addition to hCTR1 are likely involved.⁵⁶ Once in the cells, copper is processed and linked to proteins by the Golgi apparatus.^{54,56}

2.4.1 CuHARS

When configured as high-aspect ratio structures, copper has a needle-like shape with a large surface area to volume ratio. Figure 2-4 shows an image of CuHARS under brightfield microscopy. The synthesis of CuHARS from nanoparticles (CuNPs) was

initially published by the DeCoster lab, but the process has been modified since then.⁵⁷ The current method uses copper sulfate in place of CuNPs. The synthesis can be scaled up and down in volume and in amount of materials according to need.



Figure 2-4: Brightfield image of CuHARS at 100x Magnification. Scale bar = 100μm.

CuHARS are biodegradable in cell culture media.⁴ Research has also been conducted to determine the behavior of CuHARS in cell culture.⁵⁸ These studies used pheochromocytoma brain cells from rats which differ greatly from chondrocytes because cells in the brain have much larger oxygen and metabolic needs than chondrocytes as cultured in the lab.⁵⁸

CuHARS Breakdown

CuHARS were found to be stable in alcohol and water, but to break down over time in cell media.⁴ Some research has analyzed the breakdown of the structures in

astrocyte media, but that research is more qualitative than quantitative. This research aims to convert the images taken by previous researchers and turn that into usable, quantitative data that can be used to determine the breakdown rate of the CuHARS in media.

2.5 Other Cell Types

Because research indicates that chondrocytes can begin to differentiate to more of a fibroblast like cell over time, the study of other cell types is relevant.¹

2.5.1 Human Mesenchymal Stem Cells

Human mesenchymal stem cells (HMSCs) can also undergo chondrogenesis differentiation.⁵⁹ They are cells found in the bone marrow capable of differentiating into various cell types.⁶⁰ HMSCs were acquired by the lab, but ultimately not used because they lacked chondrogenic properties.

2.5.2 Astrocytes:

After discussion with the sponsor, Stone Clinic, astrocytes were chosen as a cell to study because they have long processes like chondrocytes. Per their name, astrocytes are star-shaped cells with long processes that end in peri synaptic astrocytic processes (PAPs) that communicate with synapses.⁶¹ Astrocytes support the central nervous system (CNS).⁶² They contribute to signal transmission of nerves, but they do not send the action potentials themselves.⁶² The cells play several roles within the CNS. Ultimately, astrocytes were not used in this study because of their slow proliferation rate.

Chondrocyte media and astrocyte media are similar. However, astrocyte media uses Ham's F-12K with L-Glutamine, and chondrocyte media uses DMEM 1X. The DMEM also contains L-Glutamine. The only discernable difference is that the Ham's

media contains sodium pyruvate and higher levels of amino acids.⁶³ When mixing the media, both medias have the base medium, a supplement of fetal bovine serum (FBS), and penicillin/streptomycin. However, the astrocyte media also uses horse serum, and horse serum has less growth factors within it compared to FBS.³⁷

2.5.3 Human Dermal Fibroblasts

Human dermal fibroblasts (HDFs) are the main cell type in human skin.⁶⁴ The dermal, epidermal interactions are critical for homeostasis, and the dermal fibroblasts are also key players in wound healing.⁶⁴ When participating in tissue repair, the HDFs change their behavior from proliferation to a more migratory phenotype.⁶⁴ HDFs improve skin grafts and wound healing when they are used to supplement the other cells of skin grafts.⁶⁴ Similar to chondrocytes, they produce a robust extracellular matrix (ECM) so that they can interact with epidermal cells.⁶⁴ However, in contrast to chondrocytes, the ECM of HDFs is rich in collagen types I and III instead of the collagen type II that chondrocytes create.^{5,64}

2.5.4 CRL 2303

CRL2303 cells are rat glioma cells that exhibit a morphology similar to fibroblasts.⁶⁵ Glial cells and neurons are the two categories of cells in the CNS.⁶⁶ Astrocytes, and oligodendrocytes are two of the main types of glial cells in the CNS.⁶⁶ Gliomas are brain tumors that are suspected to come from neuroglial stem or progenitor cells.⁶⁷ In the United states 6 cases of glioma per 100,000 people are diagnosed per year.⁶⁸

2.6 Research Need

The rate at which chondrocytes grow and their morphology as they age is not well understood. More in-depth research is necessary to further characterize late passage chondrocytes.

This work will use cells *in vitro* as a model to study how copper is processed and regulated in the body. The first question to be addressed is whether copper needs a carrier or any other modification to be accepted by cells. The second question is whether cartilage creation differs *in vivo* and in culture. The third question is how the CuHARS breaks down in cell media.

2.7 Hypotheses

Three specific hypotheses were tested in this study. The first is that the addition of copper to chondrocyte culture increases cartilage formation. The second is that chondrocytes proliferate at a slower rate with further passages. The third is that CuHARS break down faster in chondrocyte media than in astrocyte media.

CHAPTER 3

METHODS

Experiments were completed in three major phases: growth, proliferation research, and the collagen assay. First, the cells were grown and passaged. They were counted at various stages of growth, and media was saved for the collagen assay.

3.1 Treating Cells with CuHARS:

CuHARS were acquired from the lab supply. Once the chondrocytes were successfully thawed and passaged to the fifth passage, they were treated with $30 \frac{\mu\text{g}}{\text{mL}}$ of CuHARS and the proliferation rate and collagen production were analyzed.

3.2 Cell Culture

Adult human chondrocytes were obtained from Cell Applications (cat.#: 402-05a). The cells were grown until the fourth passage and then frozen for later use. Once thawed for use, the cells were passaged to the fifth passage and proliferation data were collected. An incubator from VWR was used to maintain the temperature at 37 °C, carbon dioxide at 5%, and oxygen at 20%. The cells were primarily cultured on VWR 12.5 cm² tissue culture flasks (North American Cat. No. 10062-870). Cell manipulations were performed under an ENVIRCO 6278C30 cell culture hood, and centrifugations were completed with a Hermle LaborTechnik GmbH - Z 323 K Universal high speed centrifuge. Reagents included DMEM (CORNING, Ref: 10-017-CV) to make cell culture media, phosphate

buffered saline (PBS) (GIBCO, Ref: 14200-075), and 0.25% Trypsin-EDTA from GIBCO supplied by ThermoFisher Scientific which lifts cells off a plate to split them.

3.3 Cell Counting Procedure:

Cell proliferation was measured by counting the cells at various time points throughout their growth. The number of cells was always known when they were plated on the flasks, and they were counted again when they were lifted for passaging. For the chondrocytes, the number of cells was also measured mid-passage.

3.3.1 Hemocytometer

After centrifuging, the cells were resuspended in media. Then, 10 μ L of the resuspended cells, and 10 μ L of trypan blue (Sigma-Aldrich, cat #T8154) were added to a PCR tube (VWR North American Cat No. 20170-012) and mixed by pipetting up and down multiple times. A second PCR tube was made with the same mixture. Next, 10 μ L of the mixture from each PCR tube was placed on each side of the hemacytometer (Hausser Scientific, Catalog No: 1483). The cells were counted in the 5 \times 5 block shown in Figure 3-1, and the cells were counted with a tally counter from VWR.

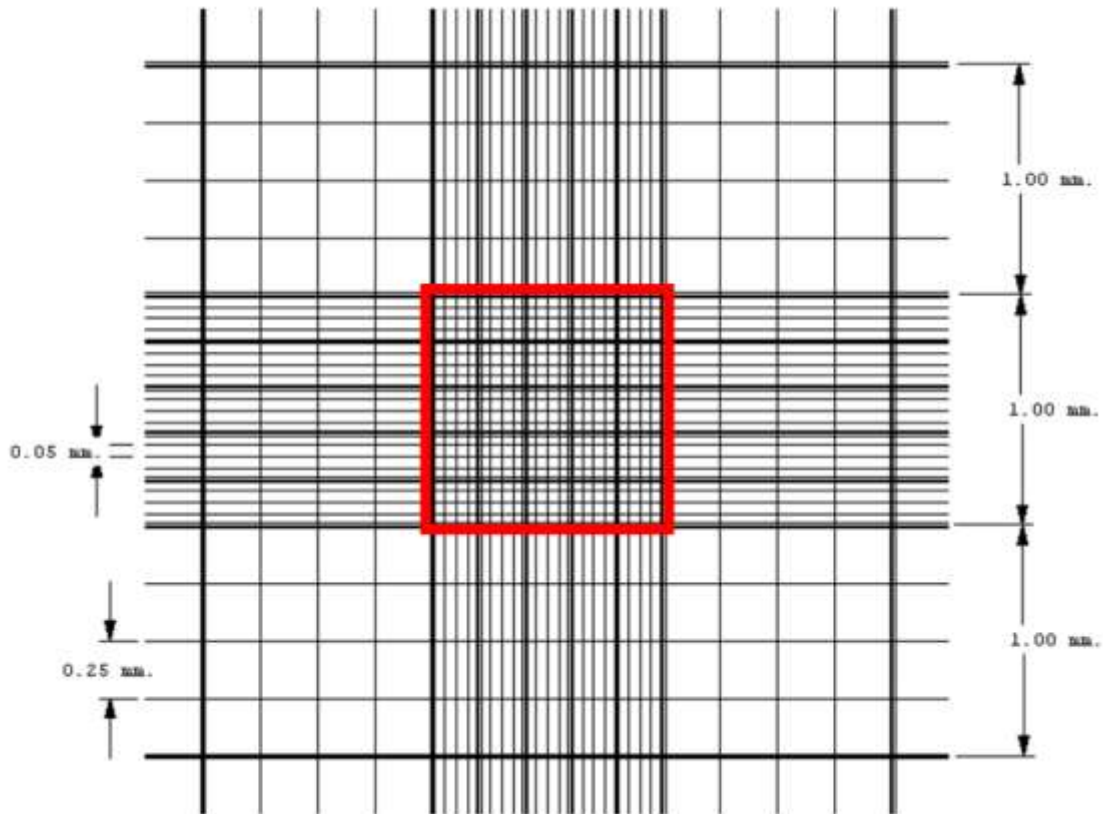


Figure 3-1: Layout of the hemacytometer with the relevant section outlined in red. ⁶⁹

The trypan blue is not absorbed by living cells, allowing them to appear bright. However, dead cells do absorb the trypan blue, causing them to appear dark blue.

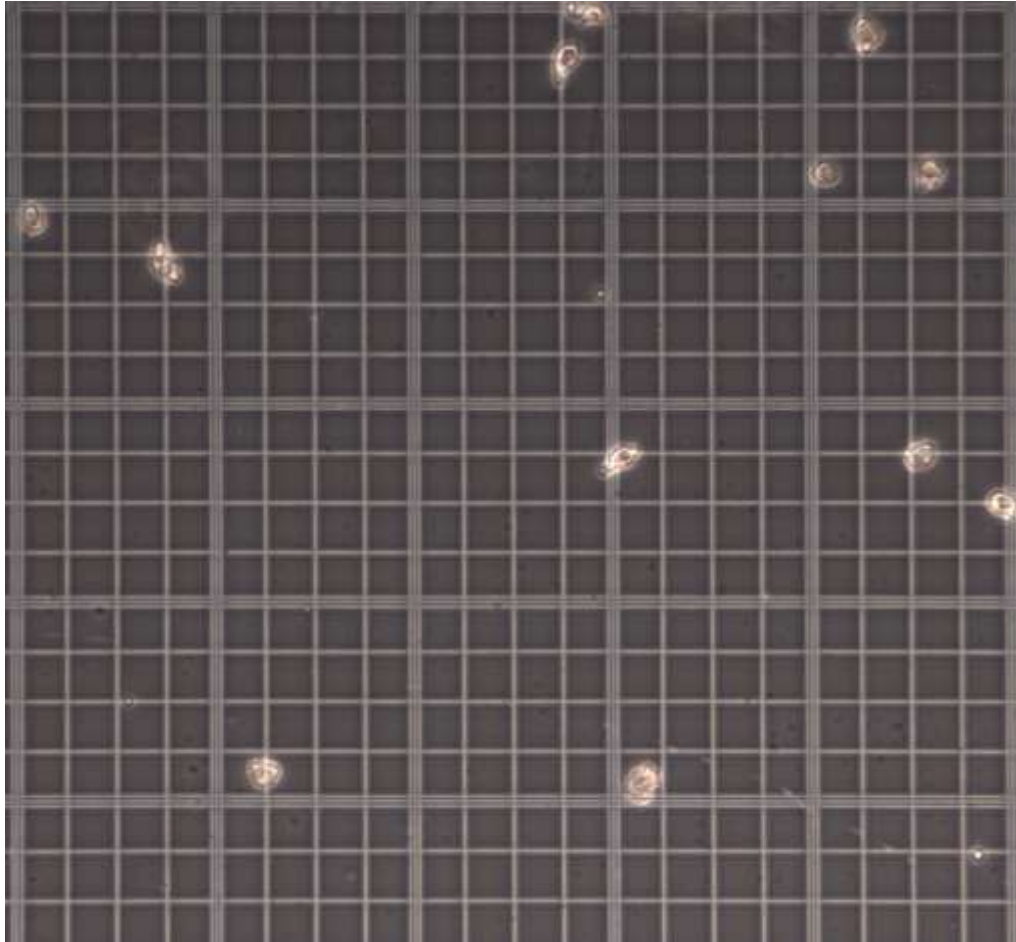


Figure 3-2: View of the hemacytometer with stained cells on it, showing high viability as no cells are stained blue.

Equation 3-1 was used to convert the counted number of cells into the suspension concentration in cells per milliliter.

$$\frac{\text{Cell Count 1} + \text{Cell Count 2}}{2} (2)(10,000) \quad \text{Equation 3-1}$$

Equation 3-1 is then multiplied by the volume of media used to resuspend the cells to get the total amount of cells in the centrifuge tube. Each time the cells were passaged, the plates were seeded with 150,000 cells with a few exceptions. In some instances when passaging the CRLs, they were seeded with 75,000 cells because they are extremely prolific.

3.3.2 Hemocytometer Control

The hemocytometer can be a useful tool in experienced hands. However, to ensure accuracy of the research, a control experiment was carried out. Beads of known size and quantity were put on the hemocytometer and counted. The beads were acquired from Thermo Scientific, formerly Duke Scientific (Cat.#35-5). They are green polystyrene beads with a measured average diameter of 24 μm . The particle density is $1.05 \frac{\text{g}}{\text{cm}^3}$. According to Equation 3-2, the volume of an individual bead was 7238.23 μm^3 .

$$\text{Volume}_{\text{sphere}} = \frac{4}{3} \pi r^3 \quad \text{Equation 3-2}$$

Equation 3-3 was used to determine the weight of each bead to further calculate how many beads are in the sample.

$$7238.23 \mu\text{m}^3 \left(\frac{1 \times 10^{-12} \text{ cm}^3}{\mu\text{m}^3} \right) \left(\frac{1.05 \text{ g}}{\text{cm}^3} \right) = 7.6 \frac{\text{ng}}{\text{bead}} \quad \text{Equation 3-3}$$

A $1 \frac{mg}{mL}$ sample was made and aliquoted into a vial. Equation 3-4 was used to determine how many beads per milliliter of water were aliquoted.

$$\frac{1 \text{ bead}}{7.6 \text{ ng}} \left(\frac{1 \text{ mg}}{\text{mL}} \right) \left(\frac{1 \times 10^6 \text{ ng}}{1 \text{ mg}} \right) \sim 131,579 \frac{\text{beads}}{\text{mL}} \quad \text{Equation 3-4}$$

Next, 10 μL of the sample and 10 μL of water were pipetted into a PCR tube before 10 μL of the solution were placed on each side of the hemocytometer. Next, the beads were counted under 100x magnification as shown in **Figure 4-11**. The total number of beads in the $1 \frac{mg}{mL}$ sample was calculated with Equation 3-1.

3.3.3 Counting cells in between passages

To better understand how the cells grew and divided in between passages, it would be impractical to lift and count the cells every day. To investigate cell proliferation, multiple techniques were attempted. First, cells were plated, then lifted from the wells every few days and counted with the hemacytometer. However, despite trying multiple volumes of trypsin, lift times, spin speeds, and plate seeding densities a consistent lift and count was not obtained from the wells.

Next, cells were imaged and counted them with computer software. After the cells were split, there were imaged every few days on a Leica DMI 6000 B microscope with a Kubler Codix light source. Leica software version 2.0 was used to power the microscope. Five images per flask were obtained on 100x magnification with phase contrast. Brightfield washed out the cells too much but was useful when imaging the CuHARS. Phase allowed for the cleanest imaging. BROAD Institute's Cell Profiler version 4.2.6 was used to count the cells mid-passage.

First, all the images were uploaded into the software. Next, the images were cropped to be 400×400 pixels for ease of processing. The RGB channels were next split to put the image into greyscale as shown in Figure 3-3.

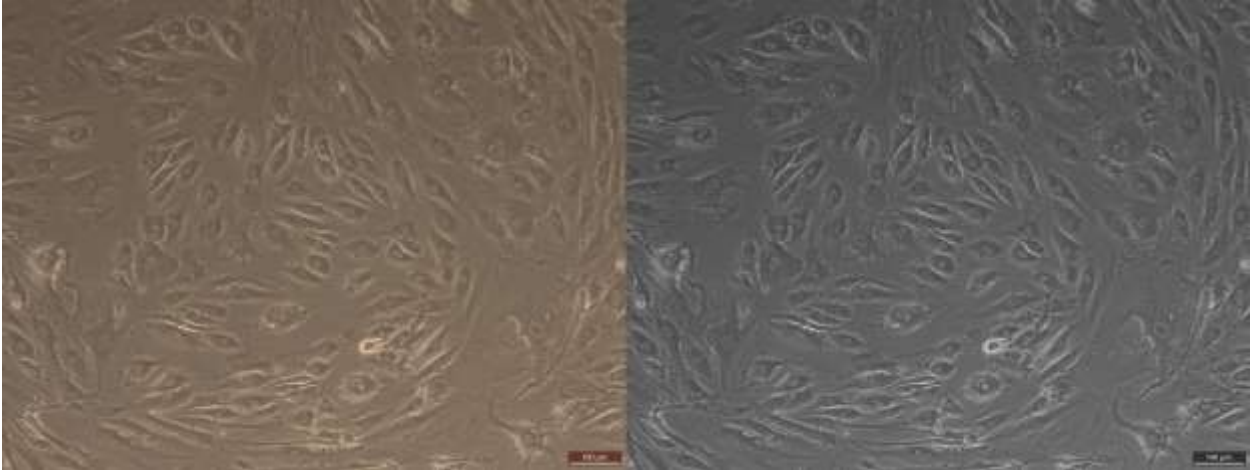


Figure 3-3: Original on the left and greyscale on the right of P10 Chondros

The red channel was then carried through the pipeline and dark holes, nuclei, of pixel size 15 to 25 pixels were enhanced to allow the nucleus to be more distinct as shown in Figure 3-4.

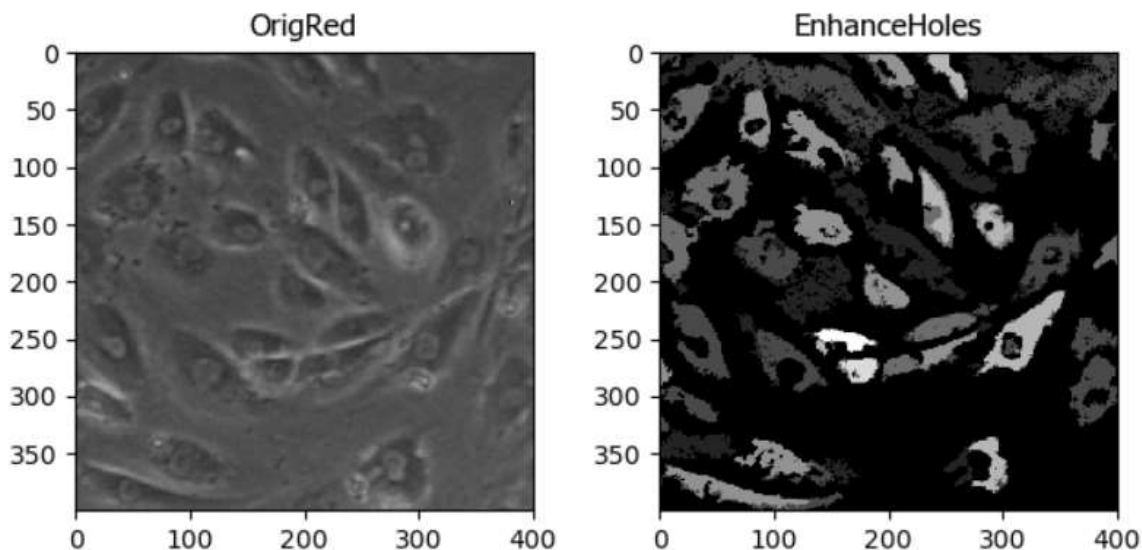


Figure 3-4: Enhanced Nuclei of Chondrocytes, showing counting success by CellProfiler.

Next, the nuclei were identified by circling the dark holes previously enhanced. The image underwent global, two-class Otsu thresholding to identify cells that were 20 pixels wide or larger. Otsu thresholding is neither parametric nor unsupervised.⁷⁰ When the two-class model is in use, it is a binary threshold model. Next, outlines were placed over the identified cells, and the cells were counted by the software. The software was instructed to ignore the borders of the image because the algorithm was inaccurate near the edges.

Finally, the results were exported to a spreadsheet and the relevant images were saved. The spreadsheet created by CellProfiler put all the results in one column, so RStudio was used to modify the Excel sheet for ease of reading. The RStudio code can be found in Appendix A.

3.3.4 HDFs

The HDF images had notably lower contrast than the chondrocytes, making it difficult for CellProfiler to differentiate between the boundaries of cells.

3.3.5 CRL2303

The CRLs are small cells. To account for their size, the original image was cropped to 200×200 pixels of the original image. Also, CRLs are so prolific that they needed to be split every four days or so. Consequently, only one set of images was taken for the CRLs as it did not feel necessary to image them as frequently because they had shorter times between passages.

3.3.6 Accuracy

The cells being measured were not stained. As a result, CellProfiler was an imperfect instrument to use because the cells had less contrast with their background as they would be had they been stained. To verify that CellProfiler was counting the cells accurately, ten images from each set were manually counted and compared to the CellProfiler results. The cropped image from CellProfiler was uploaded to OneNote for Windows 10, and the cells were circled by hand. Then, the image with the circles was uploaded to MATLAB where the circles were counted. Next, the CellProfiler and MATLAB data were compared by calculating the percentage error for each image with Equation 3-5.

$$\left| \frac{\text{Manual Count} - \text{CellProfiler Count}}{\text{Average of the 2}} (100) \right| \quad \text{Equation 3-5}$$

The percentage error was then averaged per cell type. An average percent error of 20% or lower was considered acceptable.

The code for CellProfiler was modified until it produced adequately accurate results. The counts were then exported and converted to total cells per flask. 100 μm was measured to be 110 pixels long. Each cropped image is 400 \times 400 pixels. The flasks used to culture the cells has a surface area of 12.5 cm^2 . Equation 3-6 was used to convert cells per image to cells per flask.

$$\left(\frac{\text{Cells}}{\text{image}}\right) \left(\frac{1.21 \frac{\text{pixels}^2}{\mu\text{m}^2}}{160,000 \frac{\text{pixels}^2}{\text{image}}}\right) \left(\frac{12.5 \text{ cm}^2}{\text{flask}}\right) \left(\frac{10^8 \mu\text{m}^2}{\text{cm}^2}\right) = \frac{\text{Cells}}{\text{flask}} \quad \text{Equation 3-6}$$

To simplify Equation 3-6, all of the constants were combined and multiplied by cells per image. The resulting equation is $9453.125 \frac{\text{Cells}}{\text{image}} = \frac{\text{Cells}}{\text{flask}}$.

3.4 Collagen Assay

Because collagen is important to the creation of cartilage by chondrocytes, a collagen assay kit was purchased from Sigma Aldrich to determine how much collagen was being created by the various types of cells being studied.

3.4.1 Protocol

The assay kit MAK322 (Sigma-Aldrich)¹⁰ was used to determine the amount of collagen being produced by the cells. The kit consists of a dye reagent, buffer, digestive enzyme, collagen standard, and a developer as shown in **Table 3-1**.

Table 3-1: Components of Sigma-Aldrich Collagen Assay.

Components of Kit	Catalog Number	Amount
Dye Reagent	MAK322A	5 mL
Buffer	MAK322B	5mL
Digest Enzyme	MAK322C	70 μL
Collagen Standard	MAK322D	40 μL
Developer	MAK322E	1 mL

According to the kit instructions, it is intended to perform 100 assays on 96 well plates.¹⁰ However, the protocol provided by Sigma-Aldrich was modified slightly. Only one-fourth of each standard was prepared to preserve the assay kit. When testing samples, the proportions of the master mix were maintained, but the final volume was 49 μL of mix. Whereas 450 μL of sterile water was added to ensure adequate volume in the cuvette for the spectrofluorometer to be able to read the sample.

The assay is not a radioactive one, making it safer than some other assays.¹⁰ The first step is to enzymatically digest the collagen into peptides so the N-terminal glycine peptides can bind to the dye to form a fluorescent complex.¹⁰ The samples were then put in cuvettes from Perfeq Scientific (Catalog# 9012) with 500 μL of sterile water and read from 465 nm to 499 nm wavelength with the peak at 465 nm in the F-2500 Fluorescence Spectrophotometer Model No- 251-0097. The fluorescence intensity is directly proportional to the collagen content.¹⁰

First, collagen standards were prepared according to the protocol, but with the modifications to extend the life of the assay. Table 3-2 lists the proportions of the collagen standard and water used to create the calibration curve of the assay.

Table 3-2: Collagen Standard Proportions

Tube	50 $\mu\text{g}/\text{mL}$ standard (μL)	Water (μL)	Collagen ($\mu\text{g}/\text{mL}$)
1	25	0	50
2	15	10	30
3	7.5	17.5	15
4	0	25	0

Ten μL of each standard were placed in duplicate into vials and they were labeled accordingly. The bulletin for the assay suggests diluting the samples because the assay is

meant to detect small levels of collagen.¹⁰ Samples were therefore diluted with a dilution factor of ten and placed in labeled tubes in duplicate. Next, the reaction mix was assembled consisting of a 70:1 ratio of the buffer and digestive enzyme. The protocol insists that 30 μL of the mix are necessary for each well, but 15 μL was used to extend the life of the assay. The mix was added to the vials, the plate was mixed by tapping on it, and the vials were incubated for one hour at 37 °C. Next, 20 μL of the dye reagent were added before a further 10 minutes of incubation. Four μL of the developer were added to each sample followed by another 10 minute incubation. The total volume in the vials at this point in the process was 49 μL . Four-hundred and fifty μL of water were added to ensure an adequate volume that the spectrophotometer could read. Finally, the fluorescence was measured at 375 nm excitation and 465 nm for emission.

3.4.2 Analysis

Fluorescent values from the blank sample were subtracted from those of the standard and sample values to standardize them. The adjusted standards were plotted against the concentration of collagen in the standards. The slope was calculated and used to determine the amount of collagen in each sample. For the samples, Equation 3-7 was used to account for the dilution factor.

$$\text{Collagen} \left(\frac{\mu\text{g}}{\text{mL}} \right) = \frac{F_{\text{sample}} - F_{\text{blank}}}{\text{Slope of Equation}} (\text{Dilution Factor}) \quad \text{Equation 3-7}$$

3.4.3 Accuracy

At one point, the spectrophotometer began to display similar fluorescence results for different samples. To ensure the instrument was working, fluorescein was used in several dilutions. The first set of dilutions were factors of 10, 20, and 30. Next, the first set of dilutions were treated like collagen samples. 50 μL of the fluorescein mix was

added to a further 450 μL of water. That dilution created dilution factors of 460, 470, and 480 respectively. The fluorescence of these samples was read again.

At several points in the assay, the accuracy of the instrument was a concern because the second sample often displayed a lower value than the first. So, one calibration was done, samples were run, then another calibration was carried out to check for instrument drift. Two calibration equations were created, one with each calibration. The collagen values were calculated, and the error was calculated according to Equation 3-8.

$$\text{Error} = (\text{value}_1 - \text{value}_2)^2 \quad \text{Equation 3-8}$$

Little could be done to minimize the error. It was primarily calculated to ensure it was a consistent value.

3.5 CuHARS Breakdown

Other researchers in the lab put 25 $\mu\text{g}/\text{mL}$ of CuHARS in astrocyte media and imaged the flasks every day for 18 days. The images were then imported into MATLAB where a ratio of dark pixels (CuHARS) to light pixels was calculated to determine the percent coverage of the CuHARS on the flask. The results were standardized by subtracting the number of dark pixels taken up by the scale bar. The results were then plotted against how long the CuHARS had been on the media. The code used can be found in Appendix B.

The experiment was replicated twice. The first experiment used chondrocyte media where one sample was refrigerated, one was held at room temperature, and one was kept in the incubator. The purpose was to determine the effect of temperature on the

breakdown of the material. Images were taken at day 0 and each day following until no more CuHARS could be detected by the microscope.

The results of the first replication created the need to determine the effect of the type of media on the breakdown of the material. So, one flask was astrocyte media with 25 μ g/mL CuHARS. The second flask was 25 μ g/mL of CuHARS with chondrocyte media. Images were taken at day 0 and each day following until no more HARS were detected.

The results of the second replication tested whether the CuHARS broke down faster in either media. So, the second experiment was replicated with four flasks each of astrocyte and chondrocyte media. The images were taken from day 0 to day 9 to create ten data points. The same data processing procedure was used as when only one flask was used for each medium. A paired, one-tailed t-test was then run to compare the time constants of each media.

For each replication experiment, the same MATLAB code in Appendix B was used to determine the percent coverage of the CuHARS on the flask. Once all the data were collected, a mathematical model was fit to the data. Because the data resembled an exponential decay curve, Equation 3-9 was used.

$$\% \text{ Coverage} = (x_{\text{peak}} - x_{\text{final}})e^{-\frac{t}{\tau}} + x_{\text{final}} \quad \text{Equation 3-9}$$

The following exponential fit method was applied. First, the final value was subtracted from the data set so that the adjusted data resembled a curve of the form $Ae^{-t/\tau}$. An initial value for τ was selected, and the squared error (σ^2) was calculated between the resulting model and the adjusted data at each time point.

$$\sigma^2 = (\text{Value}_{\text{model}} - \text{Value}_{\text{matlab}})^2 \quad \text{Equation 3-10}$$

The sum of these errors was then calculated, and the Solver add-in of Excel was used to find the value of τ that minimized this sum. The subtracted final value was then added back to the model equation.

CHAPTER 4

RESULTS

Immediately after synthesis, CuHARS are clumpy and comparatively large. So, they were sonicated for 5-10 minutes before the cells were treated with them. **Figure 4-1** shows the CuHARS before and after sonication.

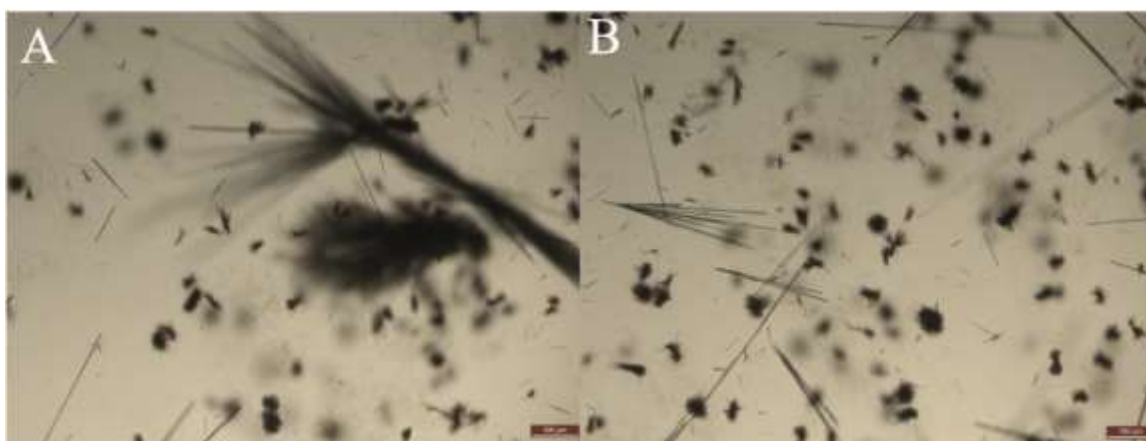


Figure 4-1: A) CuHARS prior to sonication, B) CuHARS after 5 minutes of sonication.

Sonication acts like a top-down manufacturing process that decreases the size of the material into something the cells can more readily uptake.

4.1 CuHARS Breakdown

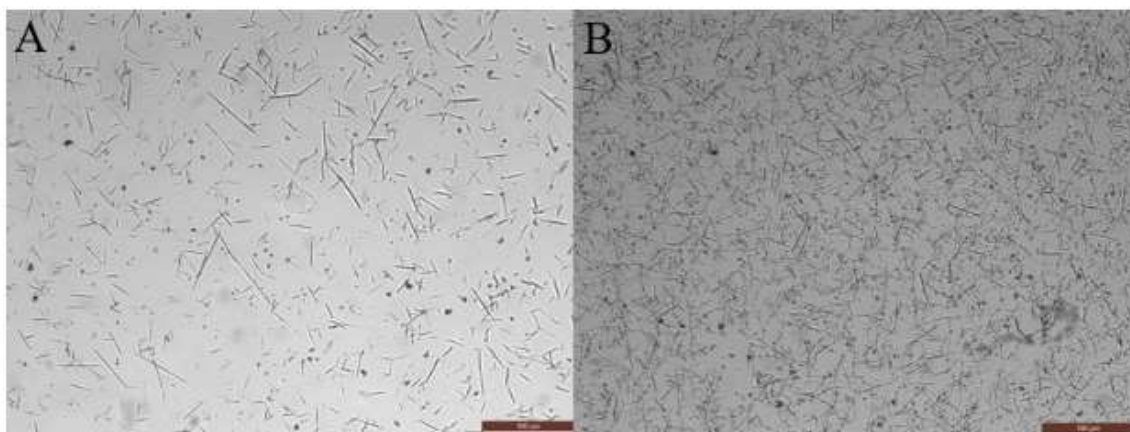


Figure 4-2 shows $25 \frac{\mu\text{g}}{\text{mL}}$ of CuHARS on astrocyte media at zero days and B is one day post treatment. The particles are smaller and appear to cover much more of the surface of the flask.

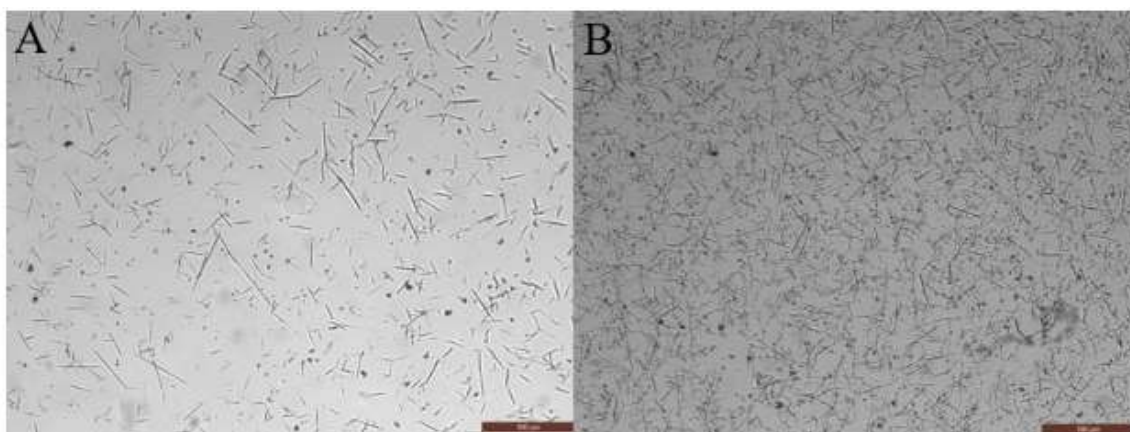


Figure 4-2: A) Day 0 CuHARS B) Day 1 CuHARS

The breakdown data were collected until there were no discernable CuHARS were visible and only particulate was observed, as seen in **Figure 4-3**.

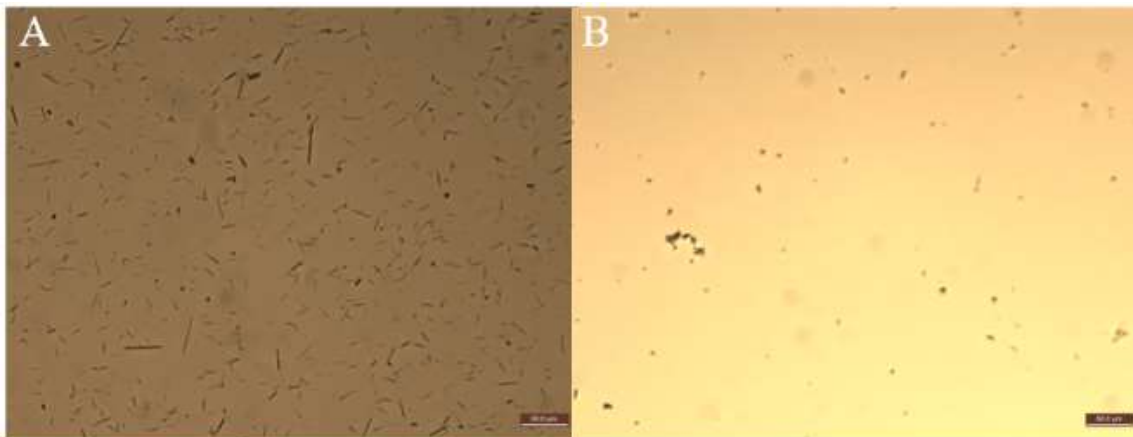


Figure 4-3: CuHARS in Astrocyte media at Day 0 (A) and Day 8 (B).

The original CuHARS breakdown data in Figure 4-4 show a peak on day one, followed by exponential decay. When the decay was modeled, a time constant of 6.7 days was determined with a least squares regression fit designed to minimize the error between the model and the data by varying the time constant.

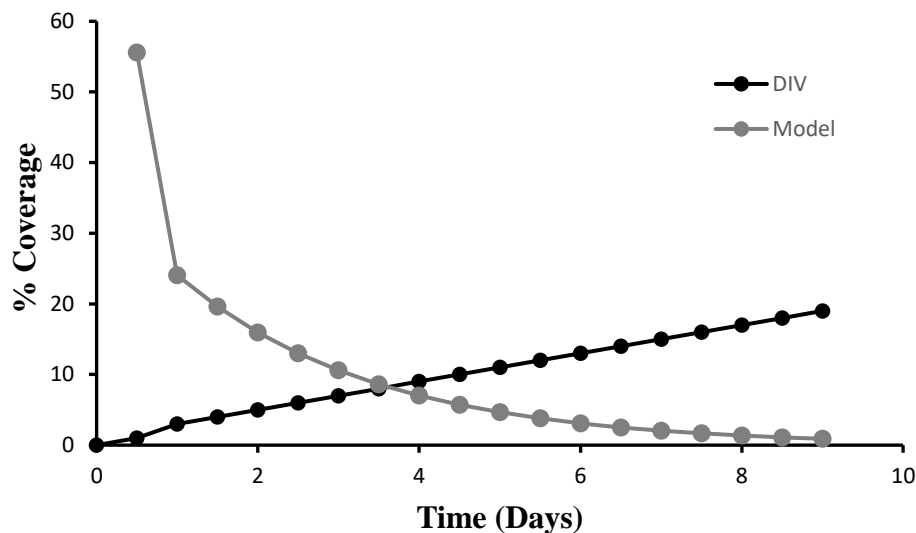


Figure 4-4: CuHARS Breakdown in Astrocyte Media.

Figure 4-5 is the result of replicating the experiment that created **Figure 4-4** but comparing the breakdown between chondrocyte and astrocyte media. The same least squares regression fit was used. Then, the time constants of the two models were compared. The time constant for the astrocyte media was 3.07 days, and the time constant for the chondrocyte media was 2.56 days. To test the statistical significance of this result, the same experiment that created **Figure 4-5** was carried was repeated with five samples for each media instead of one.

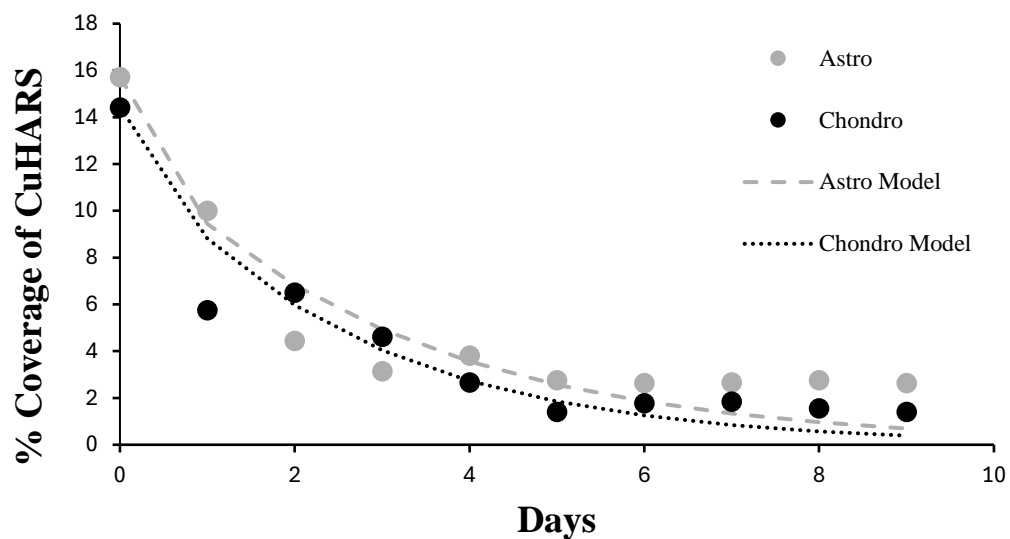


Figure 4-5: CuHARS breakdown with Astrocyte and Chondrocyte media with accompanying models.

Table 4-1 shows the time constant values for the CuHARS breakdown in astrocyte and chondrocyte media. The p-value for the paired t-test is 0.0135 indicating that the CuHARS in chondrocyte media break down faster than the CuHARS in astrocyte media. The 3rd flask of chondrocytes was infected with E. Coli and could not be used. Therefore, the outlier of the astrocyte flasks was not used. The plots for **Table 4-1: Time Constants for CuHARS breakdown in Astrocyte and Chondrocyte media.** can be found in Appendix C.

Table 4-1: Time Constants for CuHARS breakdown in Astrocyte and Chondrocyte media.

Astrocyte Tau	Chondrocyte Tau
2.97	2.39
2.39	2.05
2.75	2.56
3.28	3.02
Astrocyte Average	Chondrocyte Average
2.84	2.51
p value 0.014	

Figure 4-6 shows fifth passage chondrocytes 30 minutes post treatment with $30 \frac{\mu\text{g}}{\text{mL}}$ of CuHARS. A is the chondrocytes at 100 magnification, B is at 200 magnification with a CuHARS urchin noted to show that the image is of the same section of the flask. The CuHARS were sonicated for 10 minutes prior to their placement on the cells, so they are not difficult to see.

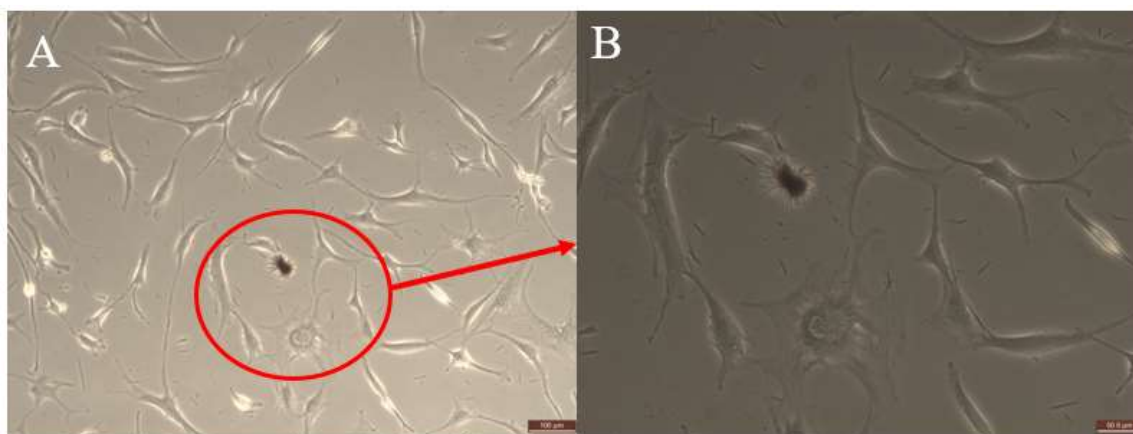


Figure 4-6: A) Chondrocytes 30 minutes post treatment at 10x, B) 20x.

Figure 4-7 A shows the chondrocytes six hours post treatment and B shows the chondrocytes three days post treatment. The CuHARS are challenging to distinguish, but

if the brightness were higher, or the images taken in brightfield, they would be more visible.

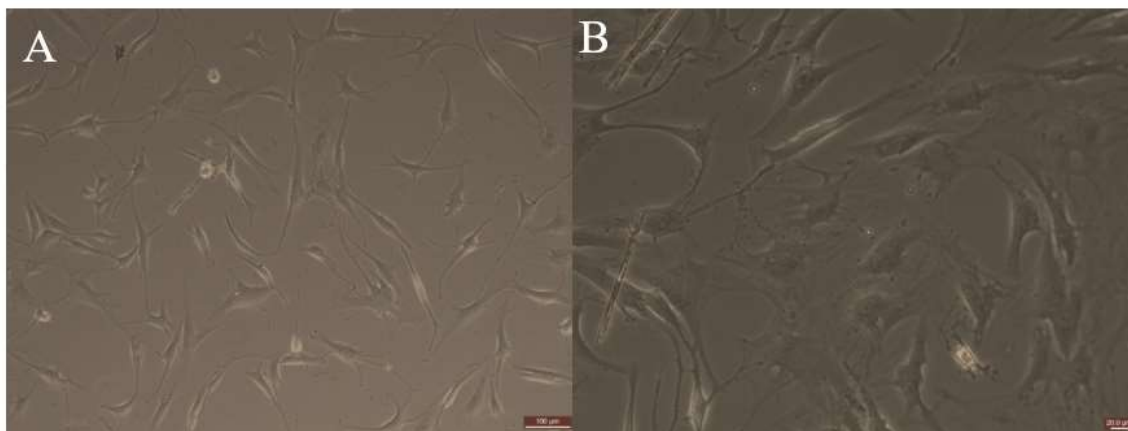


Figure 4-7: A) Chondrocytes 6hr post treatment. B) CuHARS 3 days post treatment.

Figure 4-8 is like Figure 4-7 in that A shows chondrocytes six hours after being treated with CuHARS. Panel B is an image from the same conditions as panel A but at 200x magnification so that, upon close examination, the CuHARS are visible as stick-like objects.

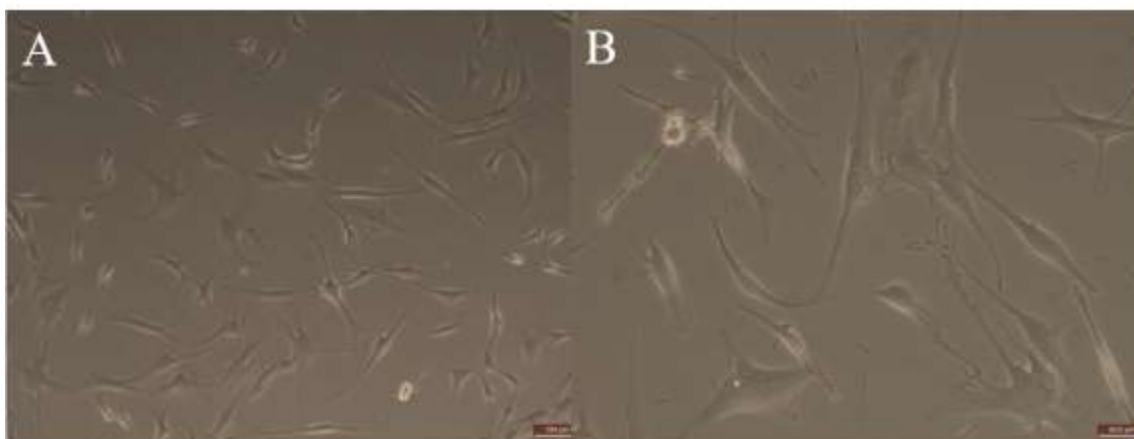


Figure 4-8: Chondrocytes 6 hours post treat 100x (A) and 200x (B).

Figure 4-9 shows image B from Figure 4-8 on a larger scale so that the CuHARS are more easily distinguishable as being inside the cells. CuHARS appear to be excluded from the cells' nuclei, which indicates that the material is inside the cell and not just laying on top of it. The larger circle is of particular interest because the CuHARS within it seem to be grouped in the processes of the cell. The three small circles show HARS that have not been taken up by the cell.

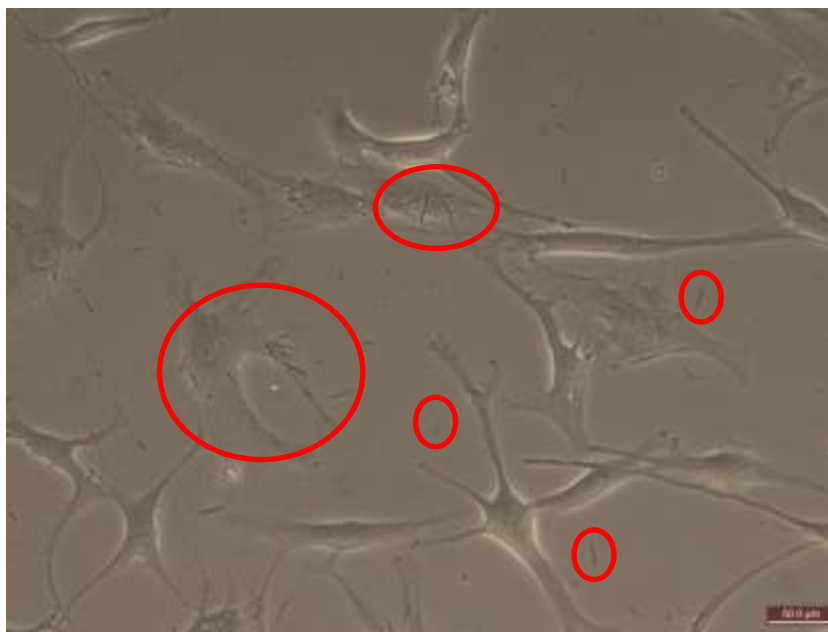


Figure 4-9: Chondrocytes 6hrs post treatment 200x. Areas of interest are circled in red.

Figure 4-10 shows the cells six days after they were treated with the CuHARS. A is the control, and B is the treated cells. The cells in B appear to be more numerous than those in image A.

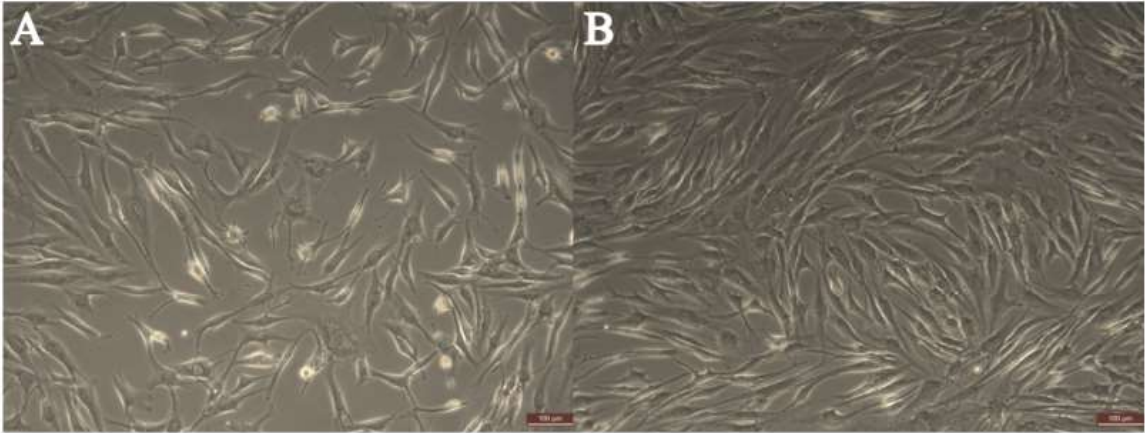


Figure 4-10: 6 days post-treatment: A) Control B) Treated

4.2 Proliferation

Figure 4-11 is an example of the calibration beads as they appear on the hemacytometer. The grid contains approximately 30 beads, which amounts to 600,000 beads per milliliter according to Equation 3-1.

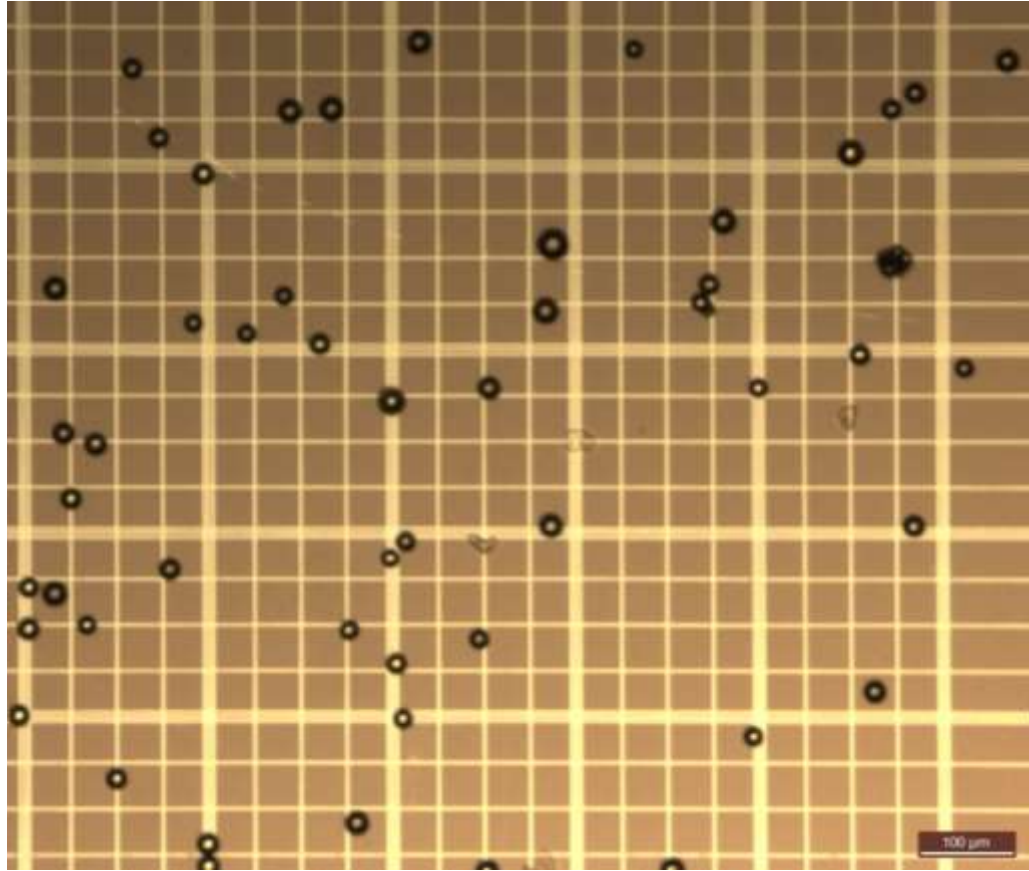


Figure 4-11: Polystyrene beads on the hemocytometer. The beads are 24 μm in diameter as per vendor specifications.

Figure 4-12 shows the output of CellProfiler including the number of cells it counted in the image. A is the greyscale, cropped image, with dark holes (nuclei) removed. B and C are cells that were identified and their outlines. D is the information on the image that CellProfiler calculated.

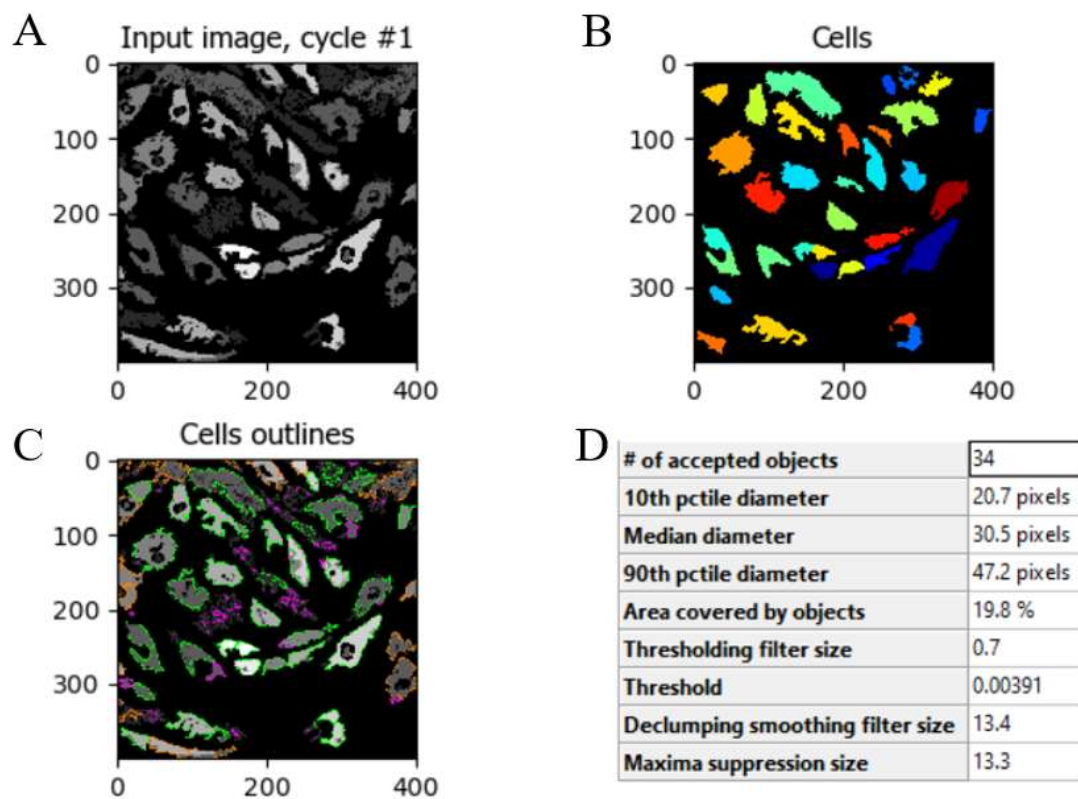


Figure 4-12: A) Greyscale of image with dark spots removed. B) Identified cells, C) Cell outlines, D) Accepted cell amount and accompanying data.

Another output of CellProfiler is **Figure 4-13** which shows the greyscale image next to the outlined cells. As evidenced by **Figure 4-13**, the system is not perfect.

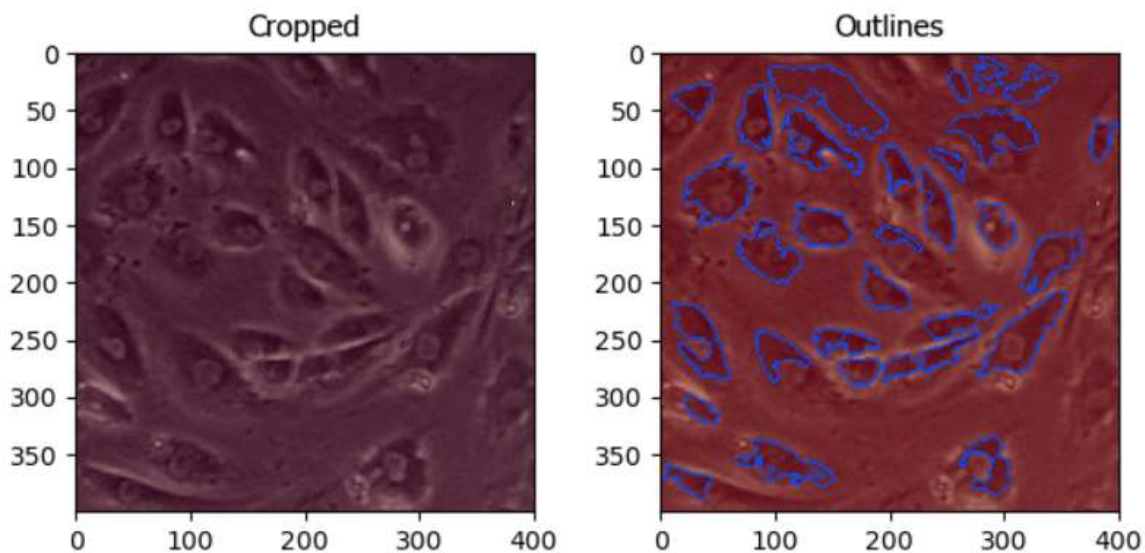


Figure 4-13: Greyscale image (Left), and the outlined cells (Right).

Figure 4-14 shows a bar chart of untreated chondrocytes, treated chondrocytes, and HDF proliferation. The untreated chondrocytes and HDFs show no discernable trend in proliferation rates. The treated chondrocytes show a general downward trend in proliferation rates as the passage number increases. The asterisk indicates a proliferation rate determined by CellProfiler. Those values are considered invalid because they are substantially smaller than the hemacytometer counts.

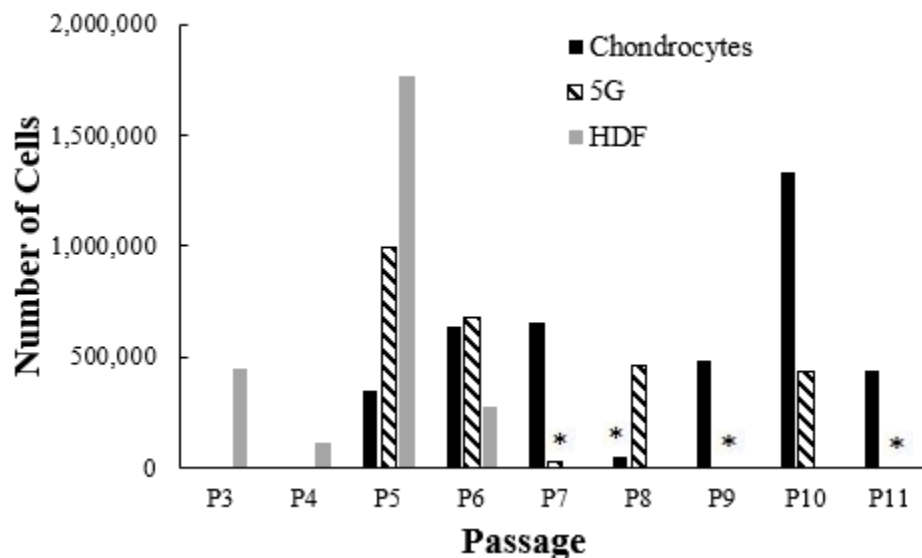


Figure 4-14: Bar Chart of Chondrocyte, Treated, and HDF Proliferation as Counted by the Hemacytometer. (* - CellProfiler Count)

Figure 4-15 shows the bar chart of how many CRL cells were created as counted by the hemacytometer. No discernable trend is detectable in the chart. If anything, CRL proliferation rates do not appear to change drastically as the passage increases.

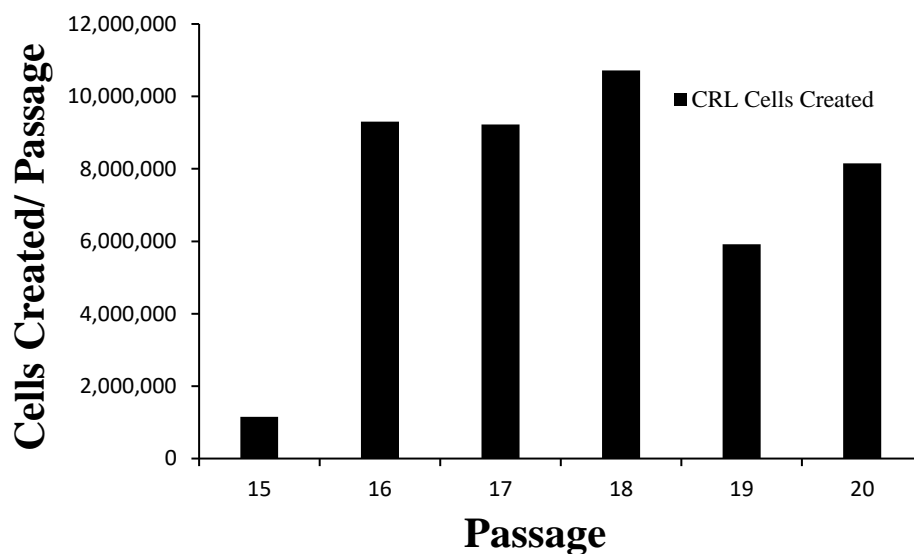


Figure 4-15: Bar Chart of CRL Proliferation

4.3 Collagen Assay

Figure 4-16 shows the calibration curve of the collagen assay. The curve is fit with a linear trendline as per the bulletin's instructions. The R^2 value is 0.96 which indicates that the trendline does not perfectly match the data. However, the data are relatively linear. Equation 3-7 was used to convert the fluorescence values to collagen content for the samples.

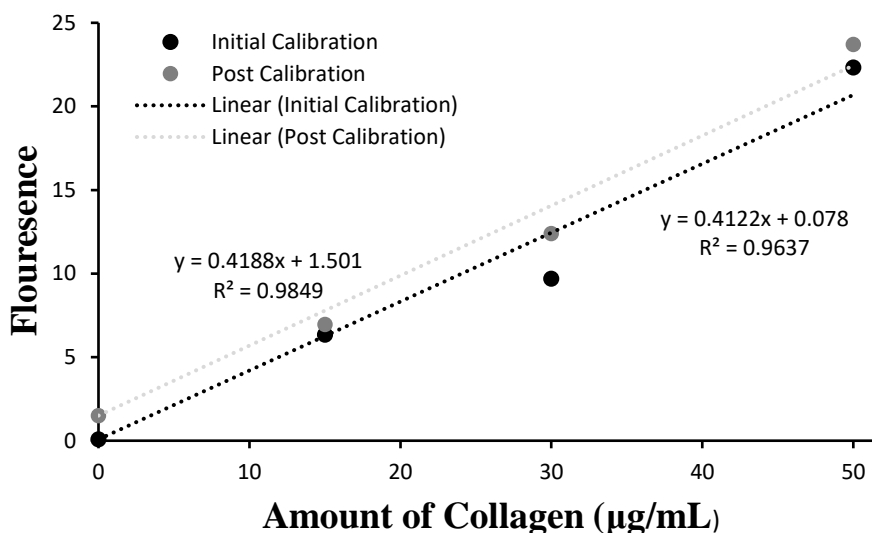


Figure 4-16: Calibration Curve of Collagen Assay.

Fluorescein was used to standardize the calibration curve. Fluorescein is highly fluorescent, and the only potential problem is that even high levels of collagen in the assay do not produce fluorescence levels that high. In **Figure 4-17**, the difference between dilution factors 10 and 20 are minimal. It is possible that fluorescein is self-quenching.

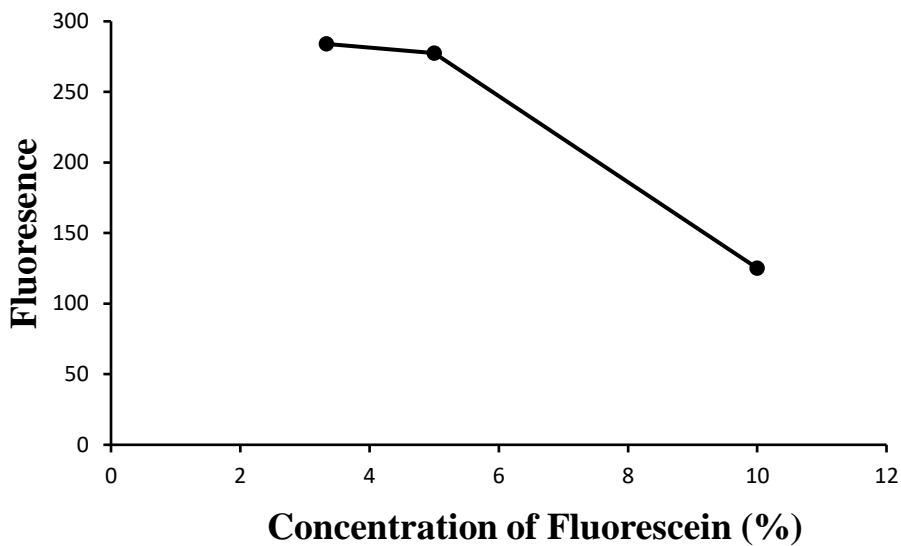


Figure 4-17: Fluorescein test at 10, 20, and 30 dilution factors

In **Figure 4-18**, it is unclear why the trendline is the exact opposite from that of **Figure 4-17**. Also, fluorescence decreases initially and then increases for no discernable reason.

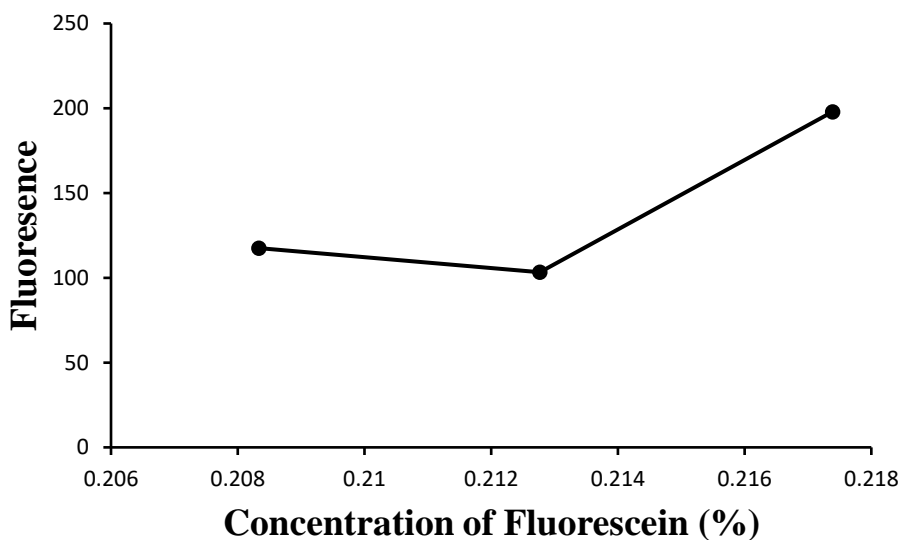


Figure 4-18: Fluorescein Test at Collagen Assay Dilutions

Figure 4-19 shows the collagen assay plot for the CRL 2303 cells. The trend in

Figure 4-19 indicates that collagen production generally decreases as the passage increases.

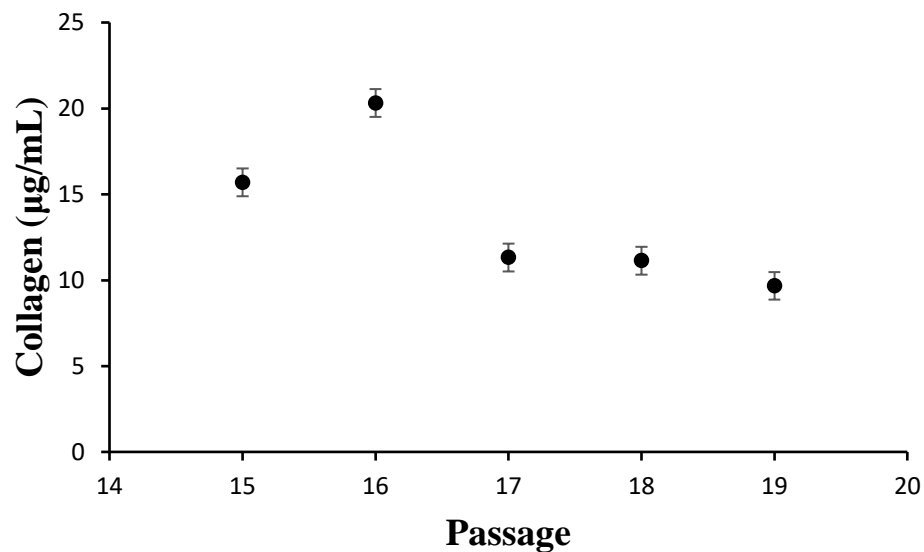


Figure 4-19: Collagen Production by CRL Cells.

Figure 4-20 shows the results of the collagen assay for the HDF cells. Generally, the trend is positive, but the three points at passage five are not as similar as expected. The culture media for the human dermal fibroblasts was switched from their own media to chondrocyte media halfway through the fifth passage. It is unknown whether that impacted the collagen production.

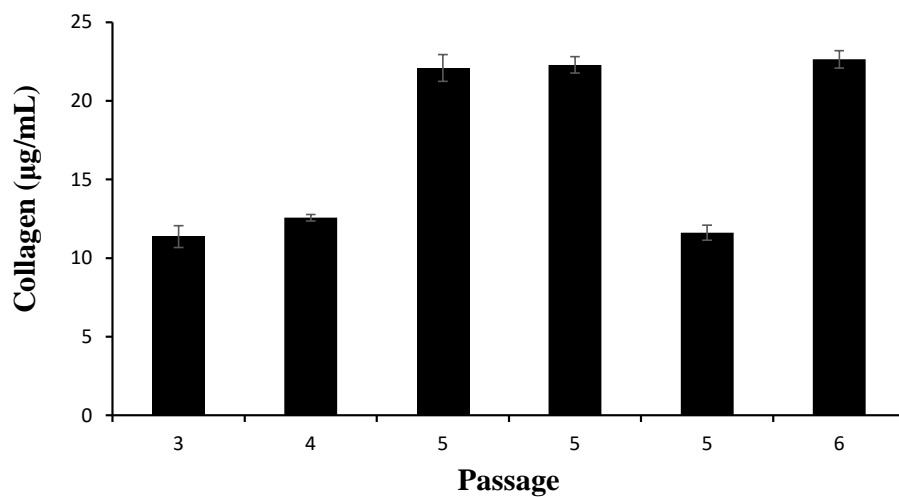


Figure 4-20: Collagen Production of Human Dermal Fibroblasts.

Figure 4-21 shows the results of the collagen assay for the treated and untreated chondrocytes. Treated chondrocytes initially made more collagen than untreated chondrocytes. After the initial treatment, it is unclear whether it makes notably more collagen until the last passage of treated chondrocytes.

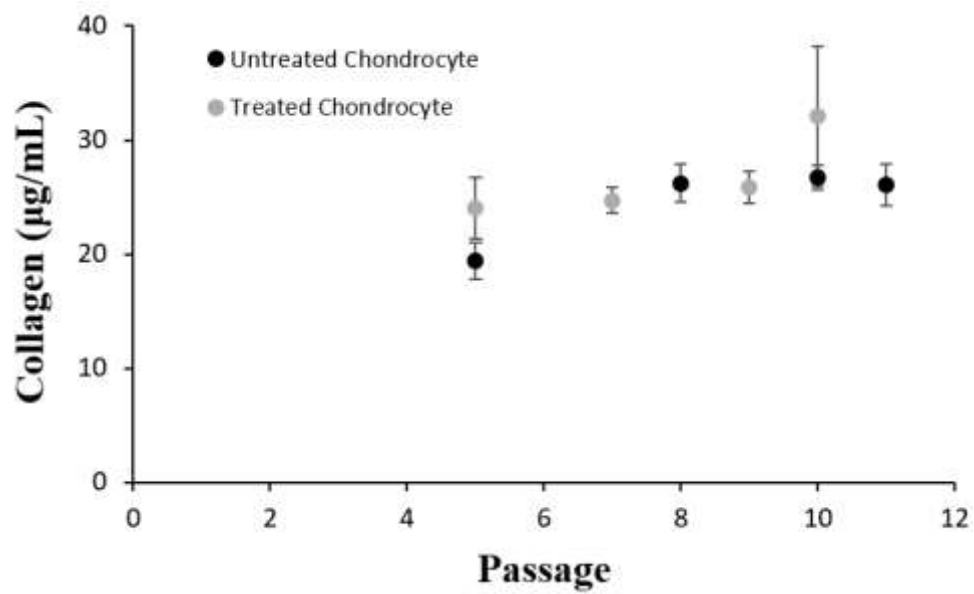


Figure 4-21: Chondrocyte and Treated Chondrocyte Collagen Production. Two data points were taken for each time point. The error bars are the difference between the two data points, divided by 2.

CHAPTER 5

DISCUSSION

It would be useful to know the breakdown rate of copper nanoparticles in various media to compare this with our novel studies here showing breakdown of CuHARS. Because the true chemical formula of CuHARS is not yet known, the mechanism by which the material breaks down or dissociates in the media cannot be deduced. Research does not seem readily available that states the solubility of copper in water because it appears stable in water, however Cuppet et al. cite it as only 0.3 mg/L at pH 7.4.⁷¹ Copper therefore cannot be dissolving as a metal in these experiments.

Karan et al. showed that the ratio of copper ions to L-cysteine, the other major component in CuHARS, is 1:1.⁷² The solubility of L-cysteine is six orders of magnitude larger, at 277 g/L⁷³, so that it might serve as a carrier for copper in the media. Important questions to answer, if the breakdown mechanism of CuHARS is to be identified, are the mode of attachment of copper to L-cysteine and the mode of attachment between L-cysteine units. One possibility is that copper is attached to the sulfur on L-cysteine, while another idea is that the copper is binding to the carboxylic acid portion of the cystine, = COO⁻, because that portion is negatively charged and the Cu⁺⁺ could then bind to two of them, helping to explain the linearity (high aspect ratio) of the material. In the future, it could be beneficial to test the media and the remaining particulate to obtain more information about the breakdown process. Another interesting experiment is to see if copper nanoparticles break down in media without the presence of cells. That

experiment would answer whether the copper was being altered by the cell media alone. The particles that appear in **Figure 4-3** may be essentially copper that remains after the breakdown of the non-copper components of the CuHARS.

In normal cell functions, copper is removed from its carrier protein, and it enters the cells alone via transport proteins. However, in the case of CuHARS, Figure 4-9 indicates that the entire structure enters the cell, which hints that a different transport mechanism may be involved instead of the normal copper pathway.

Nuclear exclusion provides evidence that the CuHARS enter the cells. Moving forward, the cells should be washed after a day or so of being treated. Washing the cells would remove excess CuHARS and provide better evidence that those remaining were in the cell. If the cells still look like they do in **Figure 4-8** after they are washed, then one could confidently say that the CuHARS are inside the cell. Alternatively, use of a confocal microscope could show conclusively that the material has entered the cell. However, a confocal microscope was inaccessible for this project.

Figure 4-11, Equation 3-1, and Equation 3-4 collectively indicate that the positive control for cell counting failed. The positive control was off by a factor of 4.56. When the positive control experiment does not produce the anticipated results, it calls into question the experiment as a whole.

Use of CellProfiler to count cells mid-passage was inaccurate and inconsistent for reasons still to be discovered. The algorithms used should have worked in theory, but they did not. A probable reason is the differences in contrast and size of the cells. For example, the HDFs had very low contrast in their images, making it nearly impossible for CellProfiler to count them. It is possible that different lighting and focus on the

microscope could aid in the issue. However, without staining the cells, perfect contrast may not be attainable. Staining the cells would have contradicted the experimentation because most stains require “fixing” or killing the cells. Therefore, to get data on the cells without killing them, most stains are not applicable. DAPI could be a good stain because it does not kill the cell and highlights the nucleus. Future work would probably benefit from experimenting with DAPI staining.

CellProfiler should have worked in theory, but it was inconsistent. The primary issue with the features used here is that they needed pronounced, round nuclei to count. The treated cells were morphologically elongated to the point where a difference in proliferation could be discerned visually, but not through the results of the software.

Figure 4-12 and **Figure 4-13** show what appear to be reasonably accurate results by the software. Most of the cells appear to be outlined and highlighted. However, the number of cells counted in the images did not correspond to the number of cells present in the flask. The results can be seen in **Figure 4-14** where the CellProfiler count was so small that it invalidated the process altogether.

The other problem with cell counting is the failure of the positive control for the hemacytometer. A hemacytometer has the potential to be a great tool within the lab. However, it appears like the research carried out here had some errors. The hemacytometer counts determined appear to be larger than those of the positive control.

Where the hemacytometer counts were too big, the CellProfiler counts were too small. There is an accurate median value somewhere between those two research methods. The untreated chondrocytes appear to yield the most precise of values, but they

are still somewhat inconsistent. For the CRLs, they are so numerous that even a slight mistake by either method could lead to massive differences in the measurement.

When replicating the CuHARS breakdown data, the peak at day one was not replicated. A third replication could help to confirm the peak values, but it is unknown whether the peak is an artifact. **Figure 4-2** shows what appears to be smaller, more numerous pieces of the CuHARS. However, during imaging while replicating the experiment, the phenomenon was not seen which raises concerns about the validity of the experiments.

The collagen assay produced mixed results. For example, the fluorescein experiment was not consistent. The fluorescein experiment was performed to demonstrate that the fluorometer was working. The inconsistency appears to arise from over-dilution of the media samples for the collagen assay. In the end, the samples were not diluted at all, and consistency improved.

The results of the collagen assay on the CRL 2303 cells are interesting. **Figure 4-15** indicates that cell proliferation does not change with the number of passages. However,

Figure 4-19 suggests that age does influence collagen production. If the outlier of passage 16 increasing age leads to a monotonic decrease in collagen production. More research into the progression of these cells is required.

The collagen assay on the human dermal fibroblasts is ultimately inconclusive as seen in **Figure 4-20** because the type of media was changed after the original media was depleted. The chondrocyte media might not have affected collagen production, but that speculation needs to be verified experimentally.

The later passages for the collagen assay on chondrocytes had consistent values, generally around 25 $\mu\text{g}/\text{m}$ (**Figure 4-21**). The treated chondrocytes ultimately made

more collagen in the latest passage. However, to demonstrate statistical significance, measurements on multiple samples must be obtained for each time point. Those measurements would require a large amount of resources.

It can be said with some confidence that only the CuHARS entered the cells, but the experiment needs to be redone with a wash to ensure loose material is removed so that any CuHARS remaining can be confidently said to be inside the cell. Only the treated cells had a discernable trend with regards to proliferation. All other cell types lack consistent trends that make sense, begging for the experiments to be repeated. The problem is that a researcher needs to go in with a solid game plan because chondrocytes take a long time to grow. CRL 2303 cells appear to show age, in that they produced less collagen at the later times, in the collagen assay, but not in proliferation data.

The experiment should be conducted again with chondrocytes that are at their second passage. Previously noted research indicates that chondrocytes start to differ in proliferation rates and morphology around passage 6. However, the chondrocytes used in this experiment were thawed at passage four and therefore could not be counted until they were passaged to the fifth passage. That, in the opinion of this researcher, did not create enough data to compare early passages to late ones.

The collagen assay had debatable reliability in these studies. The drift in the calibration curve (**Figure 4-16**) is problematic. Perhaps the dilution of the assay critically hindered the assay in some way. Fluorescein is a good positive control for the fluorometer, but it is not a good model to base measurements off of because neither **Figure 4-17** nor **Figure 4-18** showed discernable patterns that could be modeled.

It is challenging to confirm that treated cells definitively make more collagen. More research is needed in that case. However, **Figure 4-21** shows that the treated cells did make more collagen immediately after being treated. Perhaps chronically treated cells would be better for wound healing purposes.

CHAPTER 6

CONCLUSIONS AND FUTURE WORK

6.1 Conclusions

It can be said with some confidence that only the CuHARS entered the cells. The experiment needs to be redone with a wash to ensure loose material is removed so that any CuHARS remaining can be confidently said to be inside the cell.

Only the treated cells had a discernable trend with regards to proliferation. All other cell types lack trends that make sense, begging for the experiments to be repeated. These repeated experiments must be carefully planned months in advance because chondrocytes are slow-growing cells. For example, if the cells are to be chronically treated, the experimenter needs to decide when the cells are to be treated throughout their lifetime. Further, if the collagen assay were to be repeated, media would need to be saved from the earliest passage possible.

It is challenging to determine whether treated cells definitively make more collagen. More research is needed in that case. Interestingly, **Figure 4-21** shows that the treated cells did make more collagen immediately after being treated. Perhaps chronically treated cells would be better for wound healing purposes.

6.2 Future Work

CellProfiler is a potentially useful tool for counting cells mid-passage. However, the method used for this research often yielded results that were drastically lower than anticipated. DAPI staining could solve this issue in the future.

An alternative method to count cells mid-passage is a cell counter. However, cell counters use live cells within flasks, so the research would need to be started again. A cell counter could ameliorate the issue of low contrast seen in cells like the HDFs. Cell counters could also probably handle the large volume of cells seen in the CRLs. A limitation, however; is that it took almost a year to grow and passage chondrocytes enough times to collect adequate data.

Collagen assay research would benefit from expanded the effect of media. Does the media directly from cells contain enough collagen to be representative of the collagen content of the ECM? A different assay may suit the research better. Further, the Sigma Aldrich assay does not specify which type of collagen it detects. More research into the specific, notable differences of collagen type I and II could lead to the ability to differentiate between them when analyzing the cells and their extracellular matrix. Is there a way to magnify the collagen with PCR and then run a gel to see truly how much of each collagen is produced by the cells? Real-Time PCR could prove useful in this setting.

The CRL 2303 cells were not treated with the CuHARS, and they should be in the future to see if that affects collagen production, which is currently one of the few indicators that the cells are aging. Further, since the CRLs are so prolific, it is reasonable to take them through a relatively large number of passages, from early to late, in a short

amount of time. The prolific character of the CRL cells is challenging, however. The cells are less hardy than chondrocytes, so missing a day when they needed to be split could prove fatal to both the cells and the progress of the experiment.

BIBLIOGRAPHY

- (1) Caldwell, K. L.; Wang, J. Cell-Based Articular Cartilage Repair: The Link between Development and Regeneration. *Osteoarthritis and Cartilage* **2015**, *23* (3), 351–362. <https://doi.org/10.1016/J.JOCA.2014.11.004>.
- (2) Héraud, F.; Savineau, C.; Harmand, M.-F. Scandinavian Journal of Rheumatology Copper Modulation of Extracellular Matrix Synthesis by Human Articular Chondrocytes. <https://doi.org/10.1080/030097402760375179>.
- (3) Supplements, O. of D. *Copper - National Institutes of Health*; National Institutes of Health, 2022. <https://ods.od.nih.gov/factsheets/Copper-HealthProfessional/?print=1>.
- (4) Karan, A.; Darder, M.; Kansakar, U.; Norcross, Z.; DeCoster, M. A. Integration of a Copper-Containing Biohybrid (CuHARS) with Cellulose for Subsequent Degradation and Biomedical Control. *International Journal of Environmental Research and Public Health* **2018**, *15* (5), 844. <https://doi.org/10.3390/IJERPH15050844>.
- (5) Van Der Rest, M.; Garrone, R. Collagen Family of Proteins. *The FASEB Journal* **1991**, *5* (13), 2814–2823. <https://doi.org/10.1096/fasebj.5.13.1916105>.
- (6) Gupta, R. C. Chapter 13 - Nutraceuticals in Arthritis. In *Nutraceuticals*; Gupta, R. C., Ed.; Academic Press: Boston, 2016; pp 161–176. <https://doi.org/10.1016/B978-0-12-802147-7.00013-9>.
- (7) Bakilan, F.; Armagan, O.; Ozgen, M.; Tascioglu, F.; Bolluk, O.; Alatas, O. Effects of Native Type II Collagen Treatment on Knee Osteoarthritis: A Randomized Controlled Trial. *Eurasian J Med* **2016**, *48* (2), 95–101. <https://doi.org/10.5152/eurasianjmed.2015.15030>.
- (8) Qingyi, H.; Qihong, L.; Liu, Y.; Jianzhong, X. Immortalization of Human Articular Chondrocytes and Induction of Their Phenotype. *Chinese Medical Journal* **2003**, *116* (9), 1351–1356.
- (9) Fox, A. J. S.; Bedi, A.; Rodeo, S. A. The Basic Science of Articular Cartilage: Structure, Composition, and Function. **2009**. <https://doi.org/10.1177/1941738109350438>.
- (10) Mak322bul.Pdf. <https://www.sigmaaldrich.com/deepweb/assets/sigmaaldrich/product/documents/223/444/mak322bul.pdf> (accessed 2023-11-16).
- (11) Boehme, K. A.; Rolaufts, B. Onset and Progression of Human Osteoarthritis— Can Growth Factors, Inflammatory Cytokines, or Differential miRNA Expression Concomitantly Induce Proliferation, ECM Degradation, and Inflammation in

- Articular Cartilage? *International Journal of Molecular Sciences* 2018, Vol. 19, Page 2282 **2018**, 19 (8), 2282. <https://doi.org/10.3390/IJMS19082282>.
- (12) Guerne, P.; Blanco, F.; Kaelin, A.; Desgeorges, A.; Lot, M.; Guerne, P.-A.; Desgeorges, M.; Cantonal, H.; Lotz, M. Growth Factor Responsiveness of Human Articular Chondrocytes in Aging and Development. *Arthritis & Rheumatism* **1995**, 38 (7), 960–968. <https://doi.org/10.1002/ART.1780380712>.
- (13) Xia, Y.; Momot, K. I.; Chen, Z.; Chen, C. T.; Kahn, D.; Badar, F. CHAPTER 1: Introduction to Cartilage. In *Biophysics and Biochemistry of Cartilage by NMR and MRI*; Xia, Y., Momot, K. I., Eds.; New Developments in NMR; Royal Society of Chemistry, 2017; pp 3–43. <https://doi.org/10.1039/9781782623663-00001>.
- (14) Saha, S.; Kirkham, J.; Wood, D.; Curran, S.; Yang, X. B. Informing Future Cartilage Repair Strategies: A Comparative Study of Three Different Human Cell Types for Cartilage Tissue Engineering. *Cell Tissue Res* **2013**, 352 (3), 495–507. <https://doi.org/10.1007/s00441-013-1586-x>.
- (15) Armiento, A. R.; Alini, M.; Stoddart, M. J. Articular Fibrocartilage - Why Does Hyaline Cartilage Fail to Repair? *Advanced Drug Delivery Reviews* **2019**, 146, 289–305. <https://doi.org/10.1016/J.ADDR.2018.12.015>.
- (16) Kheir, E.; Shaw, D. Hyaline Articular Cartilage. *Orthopaedics and Trauma* **2009**, 23 (6), 450–455. <https://doi.org/10.1016/j.mporth.2009.01.003>.
- (17) LeBaron, R. G.; Athanasiou, K. A. Ex Vivo Synthesis of Articular Cartilage. *Biomaterials* **2000**, 21 (24), 2575–2587. [https://doi.org/10.1016/S0142-9612\(00\)00125-3](https://doi.org/10.1016/S0142-9612(00)00125-3).
- (18) Chen, H.; Tan, X.-N.; Hu, S.; Liu, R.-Q.; Peng, L.-H.; Li, Y.-M.; Wu, P. Molecular Mechanisms of Chondrocyte Proliferation and Differentiation. *Front Cell Dev Biol* **2021**, 9, 664168. <https://doi.org/10.3389/fcell.2021.664168>.
- (19) Martin, K. A.; Rzucidlo, E. M.; Ding, M.; Merenick, B. L.; Kasza, Z.; Wagner, R. J.; Powell, R. J. In Vitro Vascular Cell Culture Systems - Vascular Smooth Muscle. In *Comprehensive Toxicology, Second Edition*; Elsevier Inc., 2010; Vol. 6, pp 69–96. <https://doi.org/10.1016/B978-0-08-046884-6.00705-3>.
- (20) Kelly, T.-A. N.; Roach, B. L.; Weidner, Z. D.; Mackenzie-Smith, C. R.; O'connell, G. D.; Lima, E. G.; Stoker, A. M.; Cook, J. L.; Ateshian, G. A.; Hung, C. T. Tissue-Engineered Articular Cartilage Exhibits Tension-Compression Nonlinearity Reminiscent of the Native Cartilage. *Journal of Biomechanics* **2013**, 46, 1784–1791. <https://doi.org/10.1016/j.jbiomech.2013.05.017>.
- (21) Middendorf, J. M.; Griffin, D. J.; Shortkroff, S.; Dugopolski, C.; Kennedy, S.; Siemiatkoski, J.; Cohen, I.; Bonassar, L. J. Mechanical Properties and Structure-Function Relationships of Human Chondrocyte-Seeded Cartilage Constructs after in

- Vitro Culture. *Journal of Orthopaedic Research* **2017**, 35 (10), 2298–2306.
<https://doi.org/10.1002/JOR.23535>.
- (22) Li, S.; Oreffo, R. O. C.; Sengers, B. G.; Tare, R. S. The Effect of Oxygen Tension on Human Articular Chondrocyte Matrix Synthesis: Integration of Experimental and Computational Approaches. *Biotechnology and Bioengineering* **2014**, 111 (9), 1876–1885. <https://doi.org/10.1002/BIT.25241>.
- (23) Terry, D. E.; Chopra, R. K.; Ovenden, J.; Anastassiades, T. P. Differential Use of Alcian Blue and Toluidine Blue Dyes for the Quantification and Isolation of Anionic Glycoconjugates from Cell Cultures: Application to Proteoglycans and a High-Molecular-Weight Glycoprotein Synthesized by Articular Chondrocytes. *Analytical Biochemistry* **2000**, 285, 211–219. <https://doi.org/10.1006/abio.2000.4761>.
- (24) Schmitz, N.; Lavery, S.; Kraus, V. B.; Aigner, T. Basic Methods in Histopathology of Joint Tissues. *Osteoarthritis and Cartilage* **2010**, 18 (SUPPL. 3), S113–S116. <https://doi.org/10.1016/J.JOCA.2010.05.026>.
- (25) Dang, C.; Gilewski, T. A.; Surbone, A.; Norton, L. Cell Proliferation. In *Holland-Frei Cancer Medicine. 6th edition*; BC Decker, 2003.
- (26) Morten, B. C.; Scott, R. J.; Avery-Kiejda, K. A. Comparison of Three Different Methods for Determining Cell Proliferation in Breast Cancer Cell Lines. *J Vis Exp* **2016**, No. 115, 54350. <https://doi.org/10.3791/54350>.
- (27) Mahajan, S. D.; Law, W.-C.; Aalinkeel, R.; Reynolds, J.; Nair, B. B.; Yong, K.-T.; Roy, I.; Prasad, P. N.; Schwartz, S. A. Chapter Three - Nanoparticle-Mediated Targeted Delivery of Antiretrovirals to the Brain. In *Methods in Enzymology*; Düzgüneş, N., Ed.; Nanomedicine; Academic Press, 2012; Vol. 509, pp 41–60. <https://doi.org/10.1016/B978-0-12-391858-1.00003-4>.
- (28) Mosmann, T. Rapid Colorimetric Assay for Cellular Growth and Survival: Application to Proliferation and Cytotoxicity Assays. *Journal of Immunological Methods* **1983**, 65 (1–2), 55–63. [https://doi.org/10.1016/0022-1759\(83\)90303-4](https://doi.org/10.1016/0022-1759(83)90303-4).
- (29) Longhin, E. M.; El Yamani, N.; Rundén-Pran, E.; Dusinska, M. The Alamar Blue Assay in the Context of Safety Testing of Nanomaterials. *Frontiers in Toxicology* **2022**, 4.
- (30) *alamarBlue™ Cell Viability Reagent*.
<https://www.thermofisher.com/order/catalog/product/DAL1025> (accessed 2021-11-08).
- (31) Duronio, R. J.; Xiong, Y. Signaling Pathways That Control Cell Proliferation. *Cold Spring Harb Perspect Biol* **2013**, 5 (3), a008904.
<https://doi.org/10.1101/cshperspect.a008904>.

- (32) Schlessinger, J.; Schreiber, A. B.; Levi, A.; Lax, I.; Libermann, T.; Yarden, Y. Regulation of Cell Proliferation by Epidermal Growth Factor. *Critical Reviews in Biochemistry* **1983**, *14* (2), 93–111. <https://doi.org/10.3109/10409238309102791>.
- (33) Ornitz, D. M.; Itoh, N. Fibroblast Growth Factors. *Genome Biology* **2001**, *2* (3), reviews3005.1. <https://doi.org/10.1186/gb-2001-2-3-reviews3005>.
- (34) Dr. Wroblewski, J.; Edwall-Arvidsson, C. Inhibitory Effects of Basic Fibroblast Growth Factor on Chondrocyte Differentiation. *Journal of Bone and Mineral Research* **2020**, *10* (5), 735–742. <https://doi.org/10.1002/jbmr.5650100510>.
- (35) Ellman, M. b.; Yan, D.; Ahmadiania, K.; Chen, D.; An, H. s.; Im, H. j. Fibroblast Growth Factor Control of Cartilage Homeostasis. *Journal of Cellular Biochemistry* **2013**, *114* (4), 735–742. <https://doi.org/10.1002/jcb.24418>.
- (36) Sun, Y.; Liu, W.-Z.; Liu, T.; Feng, X.; Yang, N.; Zhou, H.-F. Signaling Pathway of MAPK/ERK in Cell Proliferation, Differentiation, Migration, Senescence and Apoptosis. *Journal of Receptors and Signal Transduction* **2015**, *35* (6), 600–604. <https://doi.org/10.3109/10799893.2015.1030412>.
- (37) Subbiahanadar Chelladurai, K.; Selvan Christyraj, J. D.; Rajagopalan, K.; Yesudhasan, B. V.; Venkatachalam, S.; Mohan, M.; Chellathurai Vasantha, N.; Selvan Christyraj, J. R. S. Alternative to FBS in Animal Cell Culture - An Overview and Future Perspective. *Heliyon* **2021**, *7* (8), e07686. <https://doi.org/10.1016/j.heliyon.2021.e07686>.
- (38) Valk, J. van der; Bieback, K.; Buta, C.; Cochrane, B.; Dirks, W. G.; Fu, J.; Hickman, J. J.; Hohensee, C.; Kolar, R.; Liebsch, M.; Pistollato, F.; Schulz, M.; Thieme, D.; Weber, T.; Wiest, J.; Winkler, S.; Gstraunthaler, G. Fetal Bovine Serum (FBS): Past – Present – Future. *ALTEX - Alternatives to animal experimentation* **2018**, *35* (1), 99–118. <https://doi.org/10.14573/altex.1705101>.
- (39) Birk, D. E.; Bruckner, P. Collagen Suprastructures. In *Collagen: Primer in Structure, Processing and Assembly*; Brinckmann, J., Notbohm, H., Müller, P. K., Eds.; Topics in Current Chemistry; Springer: Berlin, Heidelberg, 2005; pp 185–205. <https://doi.org/10.1007/b103823>.
- (40) *Collagen type-II | C106H174N32O37 | Supreme Pharmatech*. <https://supremepharmatech.com/en/process/ingredient-database/collagen-type-ii.html> (accessed 2024-03-07).
- (41) Eyre, D.; Weis, M.; Wu, J.-J. Articular Cartilage Collagen: An Irreplaceable Framework? *European cells & materials* **2006**, *12*, 57–63. <https://doi.org/10.22203/eCM.v012a07>.
- (42) Wu, Z.; Korntner, S.; Mullen, A.; Zeugolis, D. Collagen Type II: From Biosynthesis to Advanced Biomaterials for Cartilage Engineering. *Biomaterials and Biosystems* **2021**, *4*, 100030. <https://doi.org/10.1016/j.bbiosy.2021.100030>.

- (43) *Collagen type-I / alpha chain (98-110) C57H91N19O16 / Supreme Pharmatech*. <https://supremepharmatech.com/en/process/ingredient-database/collagen-type-i.html> (accessed 2024-03-07).
- (44) Grimmer, C.; Balbus, N.; Lang, U.; Aigner, T.; Cramer, T.; Mü, L.; Swoboda, B.; Pfander, D. Regulation of Type II Collagen Synthesis during Osteoarthritis by Prolyl-4-Hydroxylases Possible Influence of Low Oxygen Levels. *The American Journal of Pathology* **2006**, *169* (2). <https://doi.org/10.2353/ajpath.2006.050738>.
- (45) Antipova, O.; Orgel, J. P. R. O. In Situ D-Periodic Molecular Structure of Type II Collagen. *The Journal of Biological Chemistry* **2010**, *285* (10), 7087. <https://doi.org/10.1074/JBC.M109.060400>.
- (46) Ottani, V.; Raspanti, M.; Ruggeri, A. Collagen Structure and Functional Implications. *Micron* **2001**, *32* (3), 251–260. [https://doi.org/10.1016/S0968-4328\(00\)00042-1](https://doi.org/10.1016/S0968-4328(00)00042-1).
- (47) Miosge, N.; Hartmann, M.; Maelicke, C.; Herken, R. Expression of Collagen Type I and Type II in Consecutive Stages of Human Osteoarthritis. *Histochem Cell Biol* **2004**, *122* (3), 229–236. <https://doi.org/10.1007/s00418-004-0697-6>.
- (48) Coentro, J. Q.; Capella-Monsonís, H.; Graceffa, V.; Wu, Z.; Mullen, A. M.; Raghunath, M.; Zeugolis, D. I. Collagen Quantification in Tissue Specimens. In *Fibrosis: Methods and Protocols*; Rittié, L., Ed.; Methods in Molecular Biology; Springer: New York, NY, 2017; pp 341–350. https://doi.org/10.1007/978-1-4939-7113-8_22.
- (49) Pothen, A.-G.; Parmar, M. Fluorescein. In *StatPearls*; StatPearls Publishing: Treasure Island (FL), 2024.
- (50) PubChem. *Fluorescein*. <https://pubchem.ncbi.nlm.nih.gov/compound/16850> (accessed 2024-03-07).
- (51) *Spectrum [Fluorescein] | AAT Bioquest*. <https://www.aatbio.com/fluorescence-excitation-emission-spectrum-graph-viewer/fluorescein> (accessed 2024-03-07).
- (52) Lin, W.; Xu, L.; Li, G. Molecular Insights Into Lysyl Oxidases in Cartilage Regeneration and Rejuvenation. *Frontiers in Bioengineering and Biotechnology* **2020**, *8*, 359. <https://doi.org/10.3389/FBIOE.2020.00359/BIBTEX>.
- (53) Kumari, S.; Panda, T. K.; Pradhan, T. Lysyl Oxidase: Its Diversity in Health and Diseases. *Indian J Clin Biochem* **2017**, *32* (2), 134–141. <https://doi.org/10.1007/s12291-016-0576-7>.
- (54) Linder, M. C. Apoceruloplasmin: Abundance, Detection, Formation, and Metabolism. *Biomedicines* **2021**, *9* (3), 233. <https://doi.org/10.3390/BIOMEDICINES9030233>.

- (55) Zhou, B.; Gitschier, J. hCTR1: A Human Gene for Copper Uptake Identified by Complementation in Yeast. *Proc Natl Acad Sci U S A* **1997**, *94* (14), 7481–7486.
- (56) Kaplan, J. H.; Maryon, E. B. How Mammalian Cells Acquire Copper: An Essential but Potentially Toxic Metal. *Biophysical Journal* **2016**, *110* (1), 7–13. <https://doi.org/10.1016/j.bpj.2015.11.025>.
- (57) Kelly, K. C.; Wasserman, J. R.; Deodhar, S.; Huckaby, J.; Decoster, M. A. Generation of Scalable, Metallic High-Aspect Ratio Nanocomposites in a Biological Liquid Medium. *Journal of visualized experiments : JoVE* **2015**, *2015* (101), 1–11. <https://doi.org/10.3791/52901>.
- (58) St Marthe, K.; Karan, A.; DeCoster, M. A.; Rajendra Karekar Mount Sinai Hospital, N. BIOCOMPATIBILITY OF NOVEL COPPER-CONTAINING BIOCOMPOSITES IN QUANTIFIABLE MODEL CELL SYSTEM. **2017**.
- (59) Human Mesenchymal Stem Cells Instruction Manual Human Mesenchymal Stem Cells-Adipose-Derived (HMSC-Ad) Human Mesenchymal Stem Cells-Bone Marrow-Derived (HMSC-BM) Human Mesenchymal Stem Cells-Wharton’s Jelly-Derived (HMSC-WJ) Human Mesenchymal Stem Cells-Pre-Adipocyte (HMSC-Pre-Adipocyte).
- (60) Abdallah, B. M.; Kassem, M. Human Mesenchymal Stem Cells: From Basic Biology to Clinical Applications. *Gene Ther* **2008**, *15* (2), 109–116. <https://doi.org/10.1038/sj.gt.3303067>.
- (61) Chiareli, R. A.; Carvalho, G. A.; Marques, B. L.; Mota, L. S.; Oliveira-Lima, O. C.; Gomes, R. M.; Birbrair, A.; Gomez, R. S.; Simão, F.; Klempin, F.; Leist, M.; Pinto, M. C. X. The Role of Astrocytes in the Neurorepair Process. *Frontiers in Cell and Developmental Biology* **2021**, *9*, 1304. <https://doi.org/10.3389/FCELL.2021.665795/BIBTEX>.
- (62) Sofroniew, M. V.; Vinters, H. V. Astrocytes: Biology and Pathology. *Acta Neuropathologica* **2010**, *119* (1), 7. <https://doi.org/10.1007/S00401-009-0619-8>.
- (63) *Ham’s F-12K (Kaighn’s) Medium*. <https://www.thermofisher.com/order/catalog/product/21127022> (accessed 2024-03-07).
- (64) *Skin Tissue Engineering: Methods and Protocols*; Böttcher-Haberzeth, S., Biedermann, T., Eds.; Methods in Molecular Biology; Springer New York: New York, NY, 2019; Vol. 1993. <https://doi.org/10.1007/978-1-4939-9473-1>.
- (65) *C6/lacZ7 - CRL-2303 | ATCC*. <https://www.atcc.org/products/crl-2303> (accessed 2023-12-07).
- (66) Jessen, K. R. Glial Cells. *The International Journal of Biochemistry & Cell Biology* **2004**, *36* (10), 1861–1867. <https://doi.org/10.1016/j.biocel.2004.02.023>.

- (67) Weller, M.; Wick, W.; Aldape, K.; Brada, M.; Berger, M.; Pfister, S. M.; Nishikawa, R.; Rosenthal, M.; Wen, P. Y.; Stupp, R.; Reifenberger, G. Glioma. *Nat Rev Dis Primers* **2015**, *1* (1), 1–18. <https://doi.org/10.1038/nrdp.2015.17>.
- (68) Mesfin, F. B.; Al-Dhahir, M. A. Gliomas. In *StatPearls*; StatPearls Publishing: Treasure Island (FL), 2023.
- (69) *Metallized Hemacytometer Hausser Bright-Line*. http://www.hauserscientific.com/products/hausser_bright_line.html (accessed 2023-12-01).
- (70) Xu, X.; Xu, S.; Jin, L.; Song, E. Characteristic Analysis of Otsu Threshold and Its Applications. *Pattern Recognition Letters* **2011**, *32* (7), 956–961. <https://doi.org/10.1016/j.patrec.2011.01.021>.
- (71) Cuppett, J. D.; Duncan, S. E.; Dietrich, A. M. Evaluation of Copper Speciation and Water Quality Factors That Affect Aqueous Copper Tasting Response. *Chemical Senses* **2006**, *31* (7), 689–697. <https://doi.org/10.1093/chemse/bjl010>.
- (72) Karan, A.; Sharma, N. S.; Darder, M.; Su, Y.; Andrabi, S. M.; Shahriar, S. M. S.; John, J. V.; Luo, Z.; DeCoster, M. A.; Zhang, Y. S.; Xie, J. Copper–Cystine Biohybrid-Embedded Nanofiber Aerogels Show Antibacterial and Angiogenic Properties. *ACS Omega* **2024**, *9* (8), 9765–9781. <https://doi.org/10.1021/acsomega.3c10012>.
- (73) *The Merck Index: An Encyclopedia of Chemicals, Drugs, and Biologicals*, Fifteenth edition.; O’Neil, M. J., Ed.; Royal Society of Chemistry: Cambridge, UK, 2013.

APPENDIX A

RStudio Code

```
data.raw <- read.csv("C:\\Users\\User\\Desktop\\Cell Counting\\Cells.csv")
#directly read in file
data.raw <- data.raw[,1:3]
data <- data.frame(ImageNumber = NA, ObjectNumber = NA, FileName_DNA = NA)
for (image_num in unique(data.raw$ImageNumber)){
  x <- data.raw[data.raw$ImageNumber == image_num,]
  x <- x[x$ObjectNumber == max(x$ObjectNumber),]
  data <- rbind(data, x)
}
write.csv(na.omit(data), "C:\\Users\\User\\Desktop\\Cell
Counting\\Cells_Processed.csv", row.names = F)
x <- na.omit(data)
```

APPENDIX B

MATLAB code for CuHARS breakdown

```
%Add to path the folder with the images. The Leica produces .tif images
%The directory may need to be altered depending on file type.
clear
close all;
tifFiles = dir('*.tif');
numfiles = length(tifFiles);
mydata = cell(1, numfiles);

for k = 1:numfiles
    mydata{k} = imread(tifFiles(k).name);
    I = imread(tifFiles(k).name);
    % J = medfilt3(I);
    % K = imsharpen(J, 'Radius', 2);
    L = mat2gray(I);
    % figure('name', 'Grayscale')
    % imshow(L);
    % imshowpair(I, L, "montage")
    %imsave
    BW = imbinarize(L, 'adaptive', 'ForegroundPolarity', 'dark');
    % figure
    % imshowpair(I, BW, "montage")
    image_size = size(BW)
    binaryImage = BW > 128; % Find bright pixels instead of dark pixels.
    numDarkPixels = sum(~BW(:)); % Notice I had to invert the image with~.

    % Create a table from the outputResults matrix
    outputResults(:, k) = image_size;
    outputResults2(:, k) = numDarkPixels;

    %Have MATLAB do the calculations for me(Standardize by removing the scale
    %bar pixels
    stdpercentcoverage(:, k) = (numDarkPixels - 6431) / (1024 * 1360) * 100;
    %1024 and 1360 are the dimensions of the image. They are all the same.
end

xlswrite('CuHARS breakdown MATLAB.xlsx', {tifFiles.name}, 'Sheet1', 'A1');
%put the label of the file at the top of the Column to ensure no mix-ups
xlswrite('CuHARS breakdown MATLAB.xlsx', outputResults, 'Sheet1', 'A2');
%Parameters of the image
xlswrite('CuHARS breakdown MATLAB.xlsx', outputResults2, 'Sheet1', 'A4');
%Number of Dark Pixels
xlswrite('CuHARS breakdown MATLAB.xlsx', stdpercentcoverage, 'Sheet1', 'A5')
```

APPENDIX C

Astrocyte and Chondrocyte CuHARS Breakdown Plots

